https://doi.org/10.5194/egusphere-2023-1415
Preprint. Discussion started: 26 July 2023

Towards a mechanistic description of autoxidation chemistry: from precursors to atmospheric implications

Lukas Pichelstorfer[1,2,3], Pontus Roldin[4], Matti Rissanen[5,6], Noora Hyttinen[7], Olga Garmash[5,8], Carlton Xavier[3,4,9], Putian Zhou[3], Petri Clusius[3], Benjamin Foreback[3], Thomas Golin Almeida[3,6], Chenjuan Deng[10], Metin Baykara[3,11], Theo Kurten[6] and Michael Boy[3,12]

[1]pi-numerics, Neumarkt am W., 5202, Austria
[2]Chemistry and Physics of Materials, University of Salzburg, A-5020, Austria
[3] Institute for Atmospheric and Earth System Research/Physics, University of Helsinki, 00560 Helsinki, Finland
[4] Division of Nuclear Physics, Department of Physics, Lund University, P. O. Box 118, 221 00 Lund, Sweden
[5] Aerosol Physics Laboratory, Tampere University, 33720 Tampere, Finland
[6] Department of Chemistry, University of Helsinki, 00014 Helsinki, Finland
[7] Department of Chemistry, Nanoscience Center, University of Jyväskylä, FI-40014 Jyväskylä, Finland.
[8] Department of Atmospheric Sciences, University of Washington, Seattle, WA, USA
[9] SMHI / Swedish Meteorological and Hydrological Institute Research Department, Unit of Meteorology/Environment and Climate, SE - 601 76 NORRKÖPING
[10] State Key Joint Laboratory of Environment Simulation and Pollution Control, School of Environment, Tsinghua University, 100084 Beijing, China.
[11] Climate and Marine Sciences Department, Eurasia Institute of Earth Sciences, Istanbul Technical University, Maslak, Istanbul, 34469, Turkey
[12] School of Engineering Science, Lappeenranta-Lahti University of Technology, 53851 Lappeenranta, Finland

Correspondence to: Lukas Pichelstorfer (office@pi-numerics.com)

Abstract. In the last decades, atmospheric formation of secondary organic aerosol (SOA) gained increasing attention due to its impact on air quality and climate. However, methods to predict its abundance are mainly empirical and may fail at real atmospheric conditions. In this work, a close-to mechanistic approach allowing SOA quantification is presented, with focus on a chain-like chemical reaction called “autoxidation”. A novel framework is employed to a) describe the gas-phase chemistry, b) predict the products’ molecular structures and c) explore the contribution of autoxidation chemistry on SOA formation under various conditions. As a proof of concept, the method is applied to benzene, an important anthropogenic SOA precursor.

Our results suggest autoxidation to explain up to 100% of the benzene-SOA formed under low-NOx laboratory conditions. While under atmospheric-like day-time conditions, the calculated aerosol mass continuously increases, as expected based on prior work. Additionally, a prompt increase, driven by the NO_3 radical, is predicted at dawn. This increase has not yet been observed experimentally and questions the applicability of the widely accepted concept of OH-based SOA mass yield in the atmosphere.

https://doi.org/10.5194/egusphere-2023-1415
Preprint. Discussion started: 26 July 2023

1 Introduction

Adverse effects resulting from poor air quality nowadays represents one of the largest risks to health, causing several millions of premature deaths every year (WHO, 2021). This makes air pollution the top environmental mortality risk, e.g. much higher than polluted water (Fuller et al., 2022). In 2019, more than 99% of the global population lived in areas with outdoor PM2.5 (i.e. inhalable particles of 2.5 µm or less in aerodynamic diameter (Particulate Matter (PM) Pollution, 2022)) levels not meeting WHO guidelines (Ambient (outdoor) air pollution, 2022). In addition, while not being relevant in terms of total mass exposure, ultrafine particles (i.e., PM0.1) pose a severe health risk. After entering the body mainly through the lungs, ultrafine particles can relocate within the body to accumulate in all organs, including the brain (Schraufnagel, 2020). Occurring symptoms are systematic in nature and can be severe. The metric to quantify the hazard is, albeit being studied intensely, not fully illuminated (Shiraiwa et al., 2017). Airborne particle mass, number, and surface, as well as oxidative potential are considered to be drivers for chronic and acute effects. Recently, Daellenbach et al. have suggested that secondary organic aerosols (SOA; i.e. aerosols formed in the air from organic gaseous precursors (Hinds and Zhu, 2022)) play a major role in contributing to aerosol mass burden and, in particular, to its oxidative potential at European level (Daellenbach et al., 2020). Further, they found that ambient, respirable particular pollutants' toxicity is dominated by SOA from precursors emitted by anthropogenic activities. While primary aerosol particles impact air quality more locally and formation can be identified comparatively simply, the sources and formation pathways of SOA are complex and transport of precursor molecules can occur over large distances (Jimenez et al., 2009; Riemer et al., 2019).

In the last decade, it has been shown, mainly by means of experiment, that highly oxygenated organic molecules (HOM, as defined by Bianchi et al.(2019)) can form quickly upon oxidation of precursor volatile organic compounds (VOC) under atmospheric conditions (Bianchi et al., 2019). These, often short-lived, molecules deviate strongly from their parent VOC regarding their physical and chemical properties (Ehn et al., 2014). This particularly impacts their SOA forming potential, as the saturation vapor pressure (p_{sat}) which governs the partition to the particle phase, drops significantly with increasing functionalization of the molecules (Kroll and Seinfeld, 2008). The formation of HOM involves a key chemical process called autoxidation. It describes a chain-like process of intra-molecular H-abstractions and O_2 additions (Crounse et al., 2013; Rissanen et al., 2014). Besides the advances in experimental approaches, findings based on theoretic considerations are increasingly available (Vereecken et al., 2018; Jenkin et al., 2019; Møller et al., 2016, 2019, 2020; Vereecken and Nozière, 2020). Yet, there are few studies on deriving a mechanistic concept to predict SOA quantitatively based on the description of autoxidation chemistry under atmospheric conditions based on both: theory and experiment (Donahue et al., 2011; Roldin et al., 2019). The approach by Donahue et al.(Donahue et al., 2011), due to its formal simplicity, serves well to be applied in large scale models with substantial success. However, as the method does not aim to involve individual species but rather computes average parameters describing the evolution of gas-phase chemistry and the partition of condensable vapors to the particle phase, the authors consider it less appropriate to approach a mechanistic understanding of the oxidation process. Thus, in the present work, we follow the approach by Roldin et al. (2019), aiming for a close-to mechanistic description of

https://doi.org/10.5194/egusphere-2023-1415
Preprint. Discussion started: 26 July 2023

the autoxidation chemistry governing the process of molecular rearrangements and oxygen enrichment. We introduce the novel automated alkoxy/peroxy radical autoxidation mechanism framework ("autoAPRAM-fw" – see methods Sect. 2.1 The autoAPRAM-fw for details), capable to set up the autoxidation chemistry schemes for any VOC system. In this work, the framework is applied to benzene, a highly abundant and structurally prototypical aromatic molecule, related mainly to anthropogenic activities (Riemer et al., 2019; Han et al., 2020; Glowacki et al., 2009; Birdsall et al., 2010; Wang et al., 2017). Lately, there are also reports of the importance of biogenic emission of benzene and other BTEX species (i.e., benzene, toluene, ethylbenzene and xylenes) (Rocco et al., 2021; Misztal et al., 2015). In this work, we constrain rate coefficients of reactions related to benzene autoxidation chemistry. The approach is tested by reproducing pure gas-phase experiments and experiments investigating the SOA formation potential under high and low NO_x conditions. Further, atmospheric implications are predicted by carrying out a parameterized study computing SOA mass yields for a range of benzene and NO_x levels. Finally, atmospheric trajectory simulations are conducted to investigate the potential contribution of autoxidation chemistry and its impact on the benzene SOA evolution in the atmosphere.

2 Methods

In a first step, chemical reaction types describing benzene autoxidation chemistry are gathered from the literature (Sect. 2.2 Setting up the gas-phase chemistry). Alongside MCM(Bloss et al., 2005; Jenkin et al., 2003), a method describing basic degradation of VOC in the atmosphere, we apply the autoAPRAM-fw to add the, to date missing, depiction of benzene autoxidation chemistry (Sect. 2.1 The autoAPRAM-fw). Simulation of pure gas-phase experiments allow to constrain missing information on reaction rate coefficients (Sect. 2.3 Reaction rate coefficients). In a next step, we assign potential molecular structures to the gas-phase species formed (Sect. 2.4 The molecular structures). This is done in order to compute their saturation vapor pressures by exploring several approaches such as state-of-the-art quantum chemistry calculations or group contribution methods (Sect. 2.5 Deriving the saturation vapor pressure). In order to test the potential of the approach in predicting SOA formation, we replicate chamber experiments of benzene-OH oxidation in the presence of seed aerosol applying a detailed micro-physics and chemistry box model (Sect. 2.6 Numeric simulations: ADCHAM & ADCHEM applications). Potential atmospheric implications are illustrated in step three. At that, a parameter study on SOA yield under idealized atmospheric conditions (Sect. 2.6.4 Parametric yield study) contrasts findings from close-to realistic semi-Lagrangian atmospheric transport model calculations using ADCHEM (Sect. 2.6.3 ADCHEM & Atmospheric simulations).

2.1 The autoAPRAM-fw

The automated alkoxy/peroxy radical autoxidation mechanism framework (autoAPRAM-fw) serves to generate a model describing autoxidation chemistry of VOCs in the gas-phase. The chemistry scheme is based on MCM v3.3.1 describing the degradation of VOCs in the atmosphere (Bloss et al., 2005; Jenkin et al., 2003). The autoAPRAM-fw consists of two modules: a) autoReactions, which is applied to generate the differential equations describing autoxidation chemistry. It also

https://doi.org/10.5194/egusphere-2023-1415
Preprint. Discussion started: 26 July 2023

defines product species names and creates a computer readable chemistry model. Further, it can be used to describe functional groups of product molecules; b) autoSMILES, which creates potential structures of reaction products described by SMILE convention (Weininger, 1988). A graphical description of the framework is shown in Fig. 1.

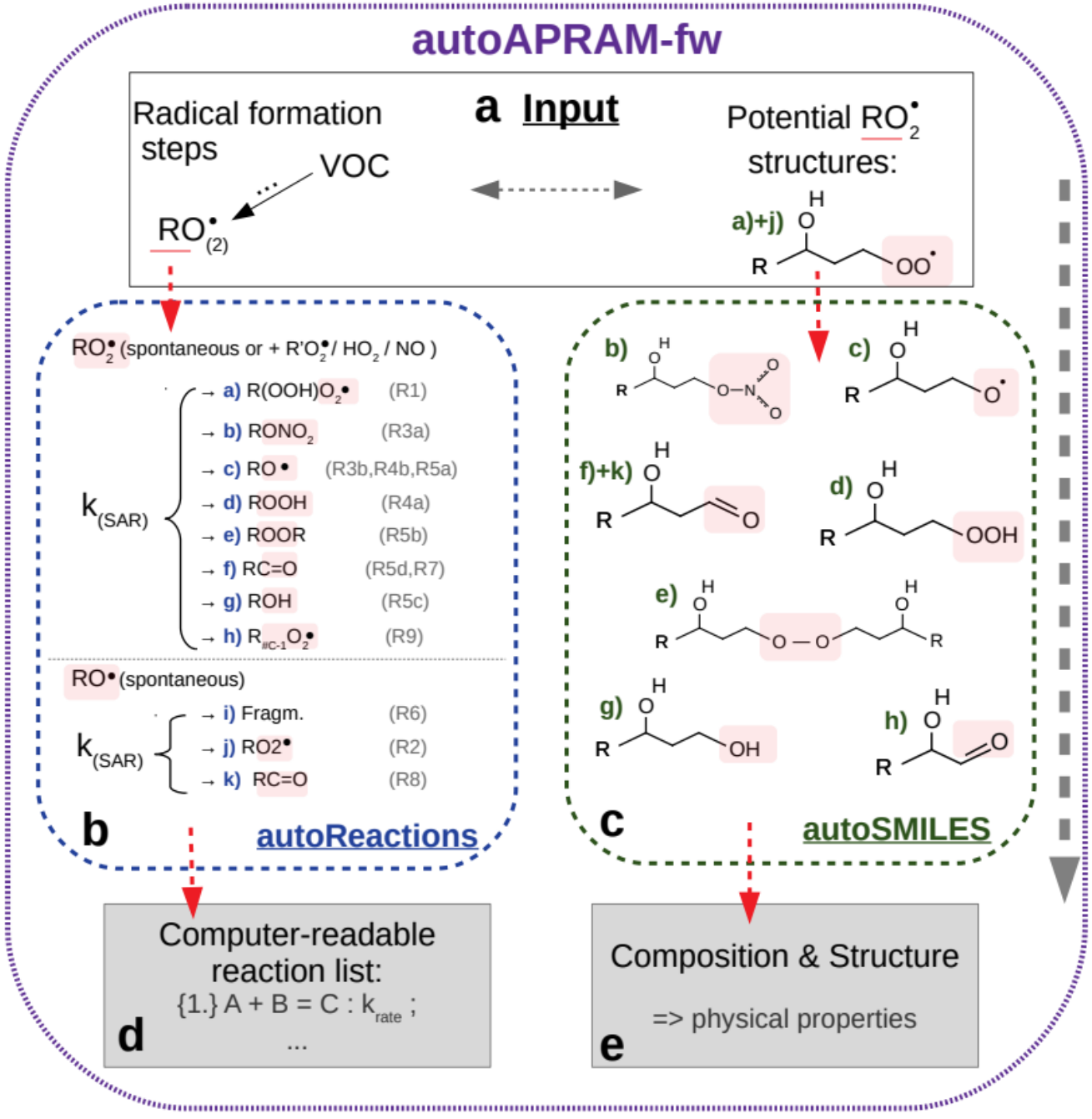

https://doi.org/10.5194/egusphere-2023-1415
Preprint. Discussion started: 26 July 2023

Fig. 1: Overview of the autoAPRAM-fw. Sector A represents the input to submodules autoReactions (B) and autoSMILES (C), respecticely. Outputs comprise a fortran readable chemistry module from autoReactions (D), and molecular information on the species formed in autoSMILES (E). Note that the submodules may be run individually.

As an input autoAPRAM-fw takes peroxy radical (RO_2) names formed in MCM together with their atomic composition. Further, RO_2 composition of species formed by autoxidation chemistry which are not described in MCM are read in. After specification of the reaction types considered, autoReactions sets up a chemical reaction scheme. Reaction rate constants can be based on theory (e.g. structure activity relationships - SAR) or can be set arbitrarily. Physical properties of the species formed can be determined from their probable structures, computed by autoSMILES, for the reaction types specified. In the present work we investigated the physical properties of product species using vapor pressure prediction methods "EVAPORATION" (Compernolle et al., 2011), "NANNOOLAL" (Nannoolal et al., 2008) and "MYRDAL/YALKOWSKI" (Myrdal and Yalkowsky, 1997) for all species, and selected species have been investigated using high performance quantum chemistry method COSMO-RS (Klamt, 1995; Klamt et al., 1998; Eckert and Klamt, 2002)).

The two modules autoReactions and autoSMILES can be run individually. The first one can be applied repeatedly to constrain the gas-phase chemistry. Note that although the model can be used to produce close to explicit gas-phase chemistry based on theory, there is still need for tuning of reaction rate constants such as branching ratios. autoSMILES may be rerun to investigate the effect of varying structures of input-RO_2 isomers. The framework itself is written in a way to describe any type of VOC undergoing autoxidation. Potentially, it can be run in an automated fashion allowing to apply machine learning techniques to tune the chemistry or investigate large numbers of RO_2 isomers.

2.2 Setting up the gas-phase chemistry

The generated gas-phase chemistry scheme is based on the master chemical mechanism (MCMv3.3.1), describing tropospheric degradation of hydrocarbons. However, MCM does not yet include autoxidation chemistry which is added by deploying the reaction types below:

$$C_zH_yO_xO_2. \xrightarrow{H-shift+O_2} C_zH_yO_{x+2}O_2. \xrightarrow{H-shift+O_2} C_zH_yO_{x+4}O_2 \quad \text{(R1)*}$$

$$C_zH_yO_xO. \xrightarrow{H-shift+O_2} C_zH_yO_{x+1}O_2. \quad \text{(R2)*}$$

$$C_zH_yO_xO_2. + NO \rightarrow C_zH_yO_xONO_2 \quad \text{(R3a)}$$

$$C_zH_yO_xO_2. + NO \rightarrow C_zH_yO_xO. + NO_2 \quad \text{(R3b)}$$

$$C_zH_yO_xO_2. + NO \rightarrow alkoxy \rightarrow C_zH_{y-1}O_xO \quad \text{(R3c)}$$

$$C_zH_yO_xO_2. + HO_2 \rightarrow C_zH_yO_xOOH \quad \text{(R4a)}$$

$$C_zH_yO_xO_2. + HO_2 \rightarrow C_zH_yO_xO. + O_2 + OH \quad \text{(R4b)}$$

https://doi.org/10.5194/egusphere-2023-1415
Preprint. Discussion started: 26 July 2023

$$C_zH_yO_xO_2.+RO_2. \rightarrow C_zH_yO_xO.+RO.+O_2 \quad \text{(R5a)}$$

$$C_zH_yO_xO_2.+RO_2. \rightarrow C_zH_yO_xOOR+O_2 \quad \text{(R5b)}$$

$$C_zH_yO_xO_2.+RO_2. \rightarrow C_zH_yO_xOH+RC=O+O_2 \quad \text{(R5c)}$$

$$C_ZH_yO_xO_2.+RO_2. \rightarrow C_ZH_{y-1}O_xO+ROH+O_2 \quad \text{(R5d)}$$

$$C_zH_yO_xO. \rightarrow fragmentation \quad \text{(R6)}$$

$$C_zH_yO_xO_2. \xrightarrow{H-shift} C_zH_{y-1}O_xO+OH/HO_2 \quad \text{(R7)*}$$

$$C_zH_yO_xO. \xrightarrow{H-shift} C_zH_{y-1}O_xO+OH/HO_2 \quad \text{(R8)*}$$

$$C_zH_yO_xO_2. \xrightarrow{H-shift} .C_zH_yO_xO_2 \rightarrow C_{z-1}H_yO_xO_2.+CO \quad \text{(R9)*}$$

Considered reaction types are described in Bianchi et al. (Bianchi et al., 2019) (reactions R1 and R2), Orlando & Tyndall (Orlando and Tyndall, 2012) (reactions R3 to R8) and Crounse et al. (Crounse et al., 2012)(reaction R9). In the current version, reactions marked with an asterisk " * " require constraining of the overall rate coefficients, while others, if applicable, require the distribution between product channels.

Upon choice of the reaction types considered, a computer readable chemistry model is created automatically by the autoAPRAM-fw. This allows to quickly set up new chemical systems, consider various atmospherically relevant SARs or to test different RO_2 isomers in a convenient way. The autoxidation chemistry connects to the MCM chemistry scheme mainly by using peroxy radicals formed in MCM.

2.3 Reaction rate coefficients

Constraining the reaction rate coefficients and branching ratios, in case of several product pathways, is neither trivial nor fully deterministic. Accordingly, potential solutions are to be expected from this method rather than the only "right answer". In the present work, the following method has proven successful. It is based on the comparison of simulated mass spectra and experimentally determined high resolution mass spectra from nitrate (NO_3^-) chemical ionization mass spectrometry (CIMS) measurements. Note that these spectra need to be interpreted with care as discussed in SI-section "Interpreting ion count data from CIMS measurements". Experimental data should be taken from well-defined experimental setups (i.e., negligible or known wall effects; well-defined precursor consumption; well known chemical systems). In the present work, we deployed flow tube experimental data, where available, for this task. The individual steps described below refer to a single specified point in time of simulation and experiment for which the chemistry code is constrained.

Step 1 is for adjusting the hydrogen shift rates in order to reproduce observed peroxy radical levels (reaction R1). This procedure has to be repeated after each of the other steps as H-shift rates interfere with the RO_2 concentrations. Peroxy

https://doi.org/10.5194/egusphere-2023-1415
Preprint. Discussion started: 26 July 2023

radicals with low oxygen number are not detected at full efficiency in NO_3^- - CIMS (Hyttinen et al., 2018). Thus, their simulated concentration may well exceed the measured.

In step 2, the rate coefficients determining dimer formation are constrained as the dimers are likely to be detected with high efficiency. Note that the least oxidized dimers may, similar to the monomers, be detected with reduced efficiency. Further, the branching ratios for RC=O (R5d) and ROH (R5c) formation are assigned. The formation of alkoxy radical is calculated based on the difference between the overall rate coefficient describing RO_2 + RO_2 and the individual closed shell forming rate coefficients determined before (reactions R5 b-d). Computing these numbers can be done best in case the RO_2 + RO_2 reactions are dominating compared to RO_2 + HO_2 or RO_2 + NO.

Step 3 comprises the determination of the branching ratio RO_2 + HO_2 → a) ROOH + O_2 or b) RO + OH + O_2 described in reactions 4a and 4b. The overall rate coefficient for RO_2 and HO_2 is obtained from MCM chemistry for the given peroxy radical. Experimental conditions where the reaction of RO2 + HO_2 is dominating (compared to RO_2 + NO or RO_2 + RO_2) is favorable to take this step. Otherwise, it is not possible to distinguish between species formed from RO_2 + RO_2 and RO_2 + HO_2 or RO_2 + NO.

Step 4 requires the determination of isomeric closed shell species formation by intramolecular hydrogen abstraction from α-hydro(pero)xyl functional groups by O_2. As a result, a carbonyl functional group is formed (reaction R7). This can be an important pathway under clean conditions, when RO_2, HO_2 and NO are not the dominating sinks of RO_2.

Step 5 is the determination of $RONO_2$ formation under high NO_x conditions (reactions R3a & R3b). Here, the NO_x level (relative to HO_2 and RO_2) is not too important as the nitrated products are distinctive (i.e., $RONO_2$ can not be confused with ROOH or ROH). This step also includes formation of alkoxy radicals that can either fragment (reaction R6), undergo RO-autoxidation to form RO_2 species (reaction R2) or form closed shell species (reaction R8). Under high NO conditions, the formation of RO_2 via RO seems to be an important path to reproduce the observed peroxy radical levels.

Elimination of CO after hydrogen abstraction from an aldehyde group is considered in step 6 (reaction R9). Resulting peroxy radicals have one less carbon atom in the chain compared to their parent VOC. For those species, steps 2 – 5 have to be repeated.

In the present work, steps 1, 2, 3, and 6 have been carried out for data from a flow tube setup. Step 5 was done for data gathered from a steady state type chamber experiment applying high NO_x levels. Due to lack of experimental data from chamber experiments representing clean conditions rate coefficients to be constrained in step 4 were estimated (i.e. low VOC reacted, low NO_x). Further, higher order RO_2 species are considered. Note that rate coefficients constrained from CIMS data to a great extent coincide with predictions from SARs for RO_2 + RO_2/HO_2/NO (Jenkin et al., 2019; Xu et al., 2020):

1) ROOR. Based on observed benzene ROOR formation and RO_2 concentrations(Molteni et al., 2018), we found the following relationship between the molecular mass of the RO_2 species and the rate coefficient:

https://doi.org/10.5194/egusphere-2023-1415
Preprint. Discussion started: 26 July 2023

$$k_{RO_2,self\,ROOR} = \begin{cases} 3.0\text{e-}13 \; if \; MM_{eff} < 334 \\ 3.\text{e-}13 + \dfrac{MM_{eff} - 334}{450 - 334} \\ 1.0\text{e-}10 \; if \; MM_{eff} > 450 \end{cases} \quad \text{equ. 1}$$

where MM_{eff} is the effective molecular mass of the reacting species (e.g., the summed atomic mass of both species). For 6 carbon containing RO_2 species, it is simply the summed molecular mass of the colliding species. For RO_2 species with 5 carbon atoms the MM_{eff} is the molecular mass + 12. Rate coefficients for ROOR formation for the self-reaction of key RO_2 species applied are plotted against nCON (i.e. the number of C, O, and N atoms in the RO_2 structure – see Jenkin et al. (2019) for more information) in Supplementary Fig S10. While the rate coefficients for RO_2 self-reaction from SAR and the dimer formation rates in autoAPRAM show a similar trend (increasing rate with increasing nCON and leveling off at a maximum value), the upper limit in the present work is higher by roughly a factor 10. However, ROOR formation rates well above 10^{-10} cm^3s^{-1} were reported recently (e.g., Berndt et al., 2018 or Molteni et al., 2019). Further, the rates from autoAPRAM show a stronger dependence on nCON. A potential reason might be a changing and unknown degree of the RO_2 (primary, secondary or tertiary) and substitution, respectively.

2) ROOH yield. While the overall rate coefficient for RO_2 + HO_2 species are adopted from MCM, the branching ratios (see reactions R4a & R4b) were constrained with experimental data. To meet the experimental findings, ROOH yields between 0.5% to 60%, with an increasing yield-trend towards higher oxidized species, are applied. For comparison, the bicyclic peroxy radical (named BZBIPERO2 in the present work), features an estimated ROOH yield of roughly 1% (Xu et al., 2020).

3) $RONO_2$ yield. Similar to the reaction R4, for the reaction RO_2 + NO (reaction R3), overall rate coefficients are obtained from MCM generic rate coefficients and branching ratios towards $RONO_2$ and RO are constrained against experimental data. Again, the alkoxy branch is dominating. $RONO_2$ yields range from 0.2% to 4% which is in line with rate coefficients reported for similar molecular structures (0.3% - 2%) (Jenkin et al., 2019; Xu et al., 2020).

2.4 The molecular structures

The autoSMILES sub-module of the autoAPRAM-fw relies on SMILES-format inputs of potential peroxy radical structures in order to compute closed shell monomer and dimer structures. However, this information is currently not available for the vast majority of the considered RO_2 species. As a consequence, an approach mainly based on theory is applied. For decades already a specific structure, the bicyclic peroxy radical (see Supplementary Fig S11), is suggested to be a key RO_2 structure that forms upon a single OH attack on benzene followed by O_2 additions (Glowacki et al., 2009; Wang et al., 2017; Xu et al., 2020; Atkinson et al., 1980). This is in line with CIMS data showing $C_6H_7O_5$ as the peroxy radical with least number of oxygen (note: odd oxygen number RO_2 with six carbon atoms; e.g. Molteni et al., 2018 or Wang et al., 2017). Accordingly, we base our considerations on this structure. To predict potential structures of other RO_2 species, we considered unimolecular rearrangements, bimolecular reactions and multiple OH attacks. The aim is to provide at least one potential

https://doi.org/10.5194/egusphere-2023-1415
Preprint. Discussion started: 26 July 2023

structure and its formation via plausible reaction paths for each peroxy radical composition detected by the mass spectrometer. The resulting formation scheme is shown in the Supplementary (Fig S12). Note that the focus of this scheme is to predict potential peroxy radical structures rather than suggesting an explicit reaction scheme. Further, radical termination pathways have been ignored in this illustration as the focus is put on radical retaining reactions. The resulting list of peroxy radical structures most likely represents only a fraction of RO_2 species involved in the autoxidation chemistry (Goldstein and Galbally, 2007).

We assume that the absence of information on RO_2 structures, from either experiment or theoretical considerations, will most likely not change in the near future. However, due to the fact that theoretical considerations are applicable to suggest structures at least for early-stage reaction products and beyond, while new technologies in mass spectrometry, such as versatile, structure specific charging technics are emerging (Hyttinen et al., 2018; Rissanen et al., 2019), we expect that this gap in knowledge will continuously decrease.

2.5 Deriving the saturation vapor pressure

The saturation vapor pressure is an important quantity to derive the partition of a species between vapor and condensed phase (Mattila et al., 1997). Ideally, it is determined experimentally. However, as the present work involves hundreds of different species, this approach is not feasible. The vapor phase molecules formed upon oxidation of precursor VOC, are characterized by their potential structures described by SMILES convention. Corresponding p_{sat} are computed by means of two different approaches: for all species, p_{sat} is derived by applying group contribution methods, namely EVAPORATION (Compernolle et al., 2011), NANNOOLAL (Nannoolal et al., 2008) and MYRDAL/YALKOWSKI (Myrdal and Yalkowsky, 1997). Group contribution methods were accessed via the online UManSysProp tool (Topping et al., 2016). Their performance is discussed in O'Meara et al. (O'Meara et al., 2014). Supplementary Fig. S13 graphically provides an overview of the volatility distribution. A few chosen molecules are investigated by means of computationally far more demanding quantum chemical calculations using the COSMO-RS model (Klamt, 1995; Klamt et al., 1998; Eckert and Klamt, 2002). This involves conformer sampling for the considered structure. The conformers showing intramolecular hydrogen bonds are removed from further analysis as they reportedly bias the results (Kurtén et al., 2018). The COSMO*conf* program (BIOVIA, COSMOconf, 2019) is used to optimize the geometries and derive the screening charge surface of each conformer considered. This forms the input for condensed phase property computation by the COSMO*therm* program (BIOVIA COSMOtherm, 2019), parameterization BP_TZVPD_FINE_19. A detailed description of the procedure can be found elsewhere (Hyttinen et al., 2022). Supplementary Fig. S14 summarizes the resulting saturation vapor pressures and their comparison to the group contribution derivates. Among the group contribution methods, EVAPORATION shows best agreement with the COSMO-RS results for all species groups (closed shell monomers, including nitrates and closed shell dimers). The inputs for the p_{sat} comparison are listed in Supplementary table ST1.

https://doi.org/10.5194/egusphere-2023-1415
Preprint. Discussion started: 26 July 2023

All SOA simulations in this work are employing the group contribution methods to describe the species' vapor pressures. In case a single SOA result is reported (i.e., for atmospheric simulations), the p_{sat} is based on EVAPORATION (Compernolle et al., 2011).

2.6 Numeric simulations: ADCHAM & ADCHEM applications

The Aerosol Dynamics gas- and particle phase chemistry model for laboratory CHAMber studies (ADCHAM; Roldin et al., 2014) and the trajectory model for Aerosol Dynamics, gas and particle phase CHEMistry and radiative transfer (ADCHEM; Roldin et al., 2019, 2011) are deployed in the present work. ADCHAM serves to compute phase change of inorganics (H_2SO_4, NH_3, HNO_3) and organics (MCM and autoAPRAM species) by considering Brownian coagulation, condensation, evaporation and dissolution. To ease computation, only condensable species with a p_{sat} lower than 1 Pa are considered to potentially partition to the particle phase. Diffusion in the carrier gas is described by Fuller's method. Detailed model inputs can be found in SI (Sect. "Model input specifications").

2.6.1 Flow tube

In the flow tube runs, potential loss of condensable vapors to the walls is considered to lie between a) zero influence and b) cross section averaged deposition to the walls for a fully developed laminar flow as described by Ingham (Ingham, 1975). These scenarios form the variation in species concentration as shown in Fig. 2 panels a, b, and c, while the center line is calculated assuming reduced loss by 50% compared to applying formulations suggested by Ingham. This is done as the flow tube comprises a laminar flow field and because reactive species are added at the center line of the flow tube to avoid the influence of the tube walls.

2.6.2 Chamber runs

ADCHAM is set up to reproduce experiments in the JPAC (Mentel et al., 2009) and the Caltech (Keywood et al., 2004) chambers, respectively. In JPAC, gas-phase oxidation of benzene in the presence of NO_x is simulated (Supplementary Fig S15) as well as under low NO_x conditions with additional seed aerosol (Fig. 3, panel a). Simulations in Caltech chamber are made for high and low NO_x conditions in the presence of seed aerosol. Note that JPAC chamber features a constant flow (into and out of the chamber) of precursors that are oxidized and removed while in Caltech chamber, the precursor concentration is highest at the start and is depleted throughout the experiment. Partition of condensable molecules between gas-phase and the chamber walls is described by considering the loss of gas-phase species i to the chamber wall, based on first order wall loss rates and, the evaporation of volatiles (i.e., species with p_{sat} higher than 10^{-7} Pa are considered in this work) from the reservoir back to the gas-phase. A detailed description of the partition formulations can be found in Roldin et al., (2019). Note that for both, the Caltech and JPAC chambers, the first order loss rates are based on experimental data. For Caltech, it is determined by Zhang et al., (2014) to be roughly 10^{-4} s^{-1} for the benzene system; in JPAC, the first order loss

https://doi.org/10.5194/egusphere-2023-1415
Preprint. Discussion started: 26 July 2023

rates are determined for $C_{10}H_{16}O_8$ (1/75 s^{-1}; see Ehn et al., 2014) and extrapolated to the species i based on the ratio of diffusion coefficient $D_i/D_{C10H16O8}$.

2.6.3 ADCHEM & Atmospheric simulations

We implemented the APRAM benzene mechanism in the chemistry transport model ADCHEM (Roldin et al., 2011, 2019) and simulated the atmospheric chemistry, aerosol dynamics and secondary organic aerosol formation downwind the Copenhagen/Malmö urban region. For a detailed description of implemented ADCHEM version the reader is referred to Roldin et al., (2019) and references therein. Specifically for the present work, ADCHEM was run along pre-calculated HYSPLIT (Rolph et al., 2017) air mass trajectories that started 7 days upwind Malmö and then continued 3 days downwind. Analogous to Xavier et al., (2022) the anthropogenic, biogenic and oceanic emissions of trace gases and primary particles were considered using CAMs global emission inventories (Granier et al., 2019) and the sea spray aerosol parameterization by Sofiev et al., (2011). The chemical mechanism, which is based on the master chemical mechanism (Jenkin et al., 1997; Saunders et al., 2003; Jenkin et al., 2015) also include the monoterpene PRAM mechanism (Roldin et al., 2019), a novel dimethyl sulfide (DMS) multiphase chemistry mechanism (Wollesen de Jonge et al., 2021) and the APRAM benzene mechanism from the present work. We selected three air mass trajectories which arrived in Malmö before noon on April 28, 2021 ("9 am", "10 am" or "11 am" local wintertime (UTC + 1 hour)), continued over Copenhagen, pass over Northern Danish agricultural region in the afternoon/night and then spent >2 days over the North Sea before the air mass was transported inland over the harbour and urban regions of Antwerp and Brussels. The selected cases demonstrate how the benzene radical chemistry and SOA formation change upon several consecutive daytime and nighttime cycles with surface layer NO_x levels ranging from ~30 ppb_v over Copenhagen to ~70 ppt over the North Sea.

In this work, the third case, "11 am", is discussed in detail. Plots showing respective results for the cases "9 am" and "10 am" can be found in the SI. Data are discussed from 1 days upwind to 3 days downwind Malmö, except for the air mass trajectories (full trajectories over the 10 days simulation period are given by Supplementary Fig. S1). The simulation days 7 to 1 days upwind are applied to allow a buildup of the gas-phase species.

2.6.4 Parametric yield study

Aiming to provide an overview of possible benzene mass yield values, we conducted a series of numerical simulations under atmospheric-like, daytime conditions. Mass yield, in this context, refers to maximum observed mass yield under predefined conditions as is typically reported in the literature (e.g., Ng et al., 2007). Briefly, OH attacks benzene, leading to the formation of peroxy radicals. Those can undergo autoxidation to form condensable material accumulating on the seed aerosol. The presence of other VOC species, represented by methane and NO interferes with the autoxidation process as recently shown by McFiggans et al., (2019).

Detailed information on the approach can be found in the supplementary information section "Description of parametric yield calculations". Supplementary table ST2 provides an overview of the inputs.

https://doi.org/10.5194/egusphere-2023-1415
Preprint. Discussion started: 26 July 2023

3 Results

3.1 Pure gas-phase simulations

The applied chemistry scheme is set up by coupling the basic description of tropospheric benzene degradation, obtained from master chemical mechanism (MCM; see Methods section for details), to the autoxidation chemistry scheme created by the autoAPRAM-fw. Missing reaction rate coefficients are constrained based on flow tube and chamber experiments. MCM describes the degradation of VOC species including the formation of peroxy radicals which produce oxygenated closed shell species by unimolecular or bimolecular reactions. Multiple generations of oxidations are considered. Thermodynamically more stable fragmentation products build up via the alkoxy radical paths, ultimately forming CO and CO_2 (Bloss et al., 2005; Jenkin et al., 2003). Formally, the autoAPRAM-fw adds the formation of high oxygen containing species by considering autoxidation chemistry in addition to the MCM chemistry scheme. Besides various closed shell product forming reactions, autoxidation (most likely consisting of an intramolecular hydrogen abstraction followed by the addition of O_2) of peroxy- (RO_2) and alkoxy- (RO) radicals is the key process. Implementing the combined chemistry scheme into the aerosol dynamics model ADCHAM (Roldin et al., 2014) enables computational reproduction of pure gas-phase experiments focusing on autoxidation.

Computer simulations of a flow tube setup employed by Molteni et al., (2018) show the applicability of the approach (Fig. 2, panels a-d; dimer concentrations were raised by factor 2 for better visibility). Note that monomers refer to reaction products having the same or smaller carbon number compared to the VOC precursor. Dimers form by the accretion reaction of monomer-radicals. Variation of the results comes from diffusive losses and is described in detail in the methods section (see Sect. 2.6 Numeric simulations: ADCHAM & ADCHEM applications). As depicted by panel a, the model is able to reproduce the atomic mass distribution measured by means of nitrate chemical ionization mass spectrometer (NO_3^- - CIMS). Further, the monomer to dimer ratio and the radical distribution are reproduced (Fig 2, panels c and d). Deviation of modeled and experimental concentration is observed for the least oxygenated peroxy radicals and their closed shell derivatives (i.e., species with molecular mass below 180 amu; without reagent ion), excluding dimers (panel a). This, however, is not surprising as the detection efficiency of these species is lowered due to their structural specifications (Hyttinen et al., 2018).

https://doi.org/10.5194/egusphere-2023-1415
Preprint. Discussion started: 26 July 2023

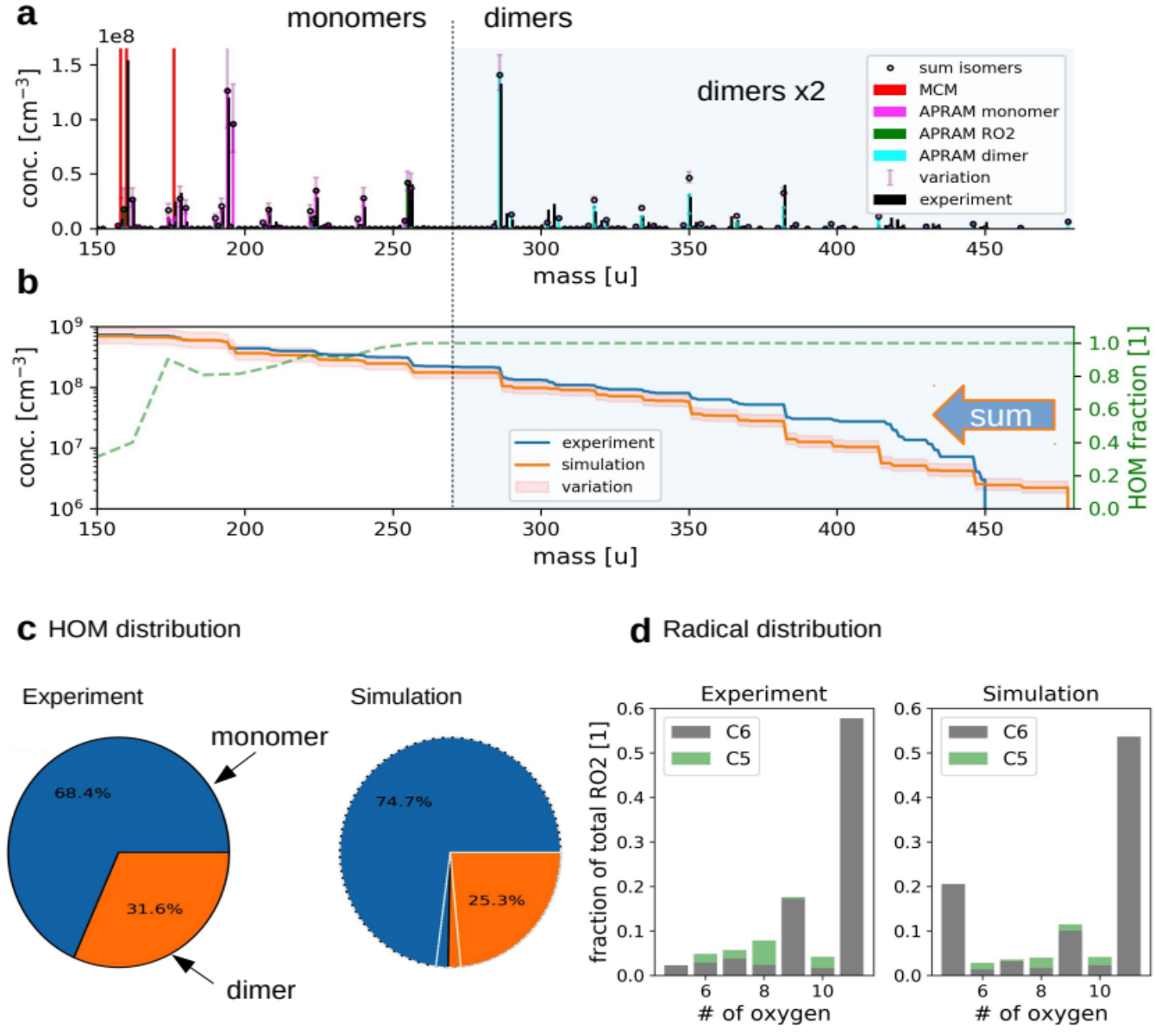

Fig. 2 summarizes the simulation of OH oxidation of benzene in the presence of UV light. Panel a depicts the gas-phase molecular mass distribution from flow tube experiment (Molteni et al., 2018) (black bars) and the simulation results (colored bars show the concentrations of individual species; "sum isomers" represents the sum of simulated isomers; note that dimer concentrations are raised by a factor of 2 to increase readability). Panel b shows cumulative representation of the model results, starting at the upper observed molecular mass limit. The secondary axis indicates the computed HOM fraction. Panel c depicts the distribution of HOM species between the monomers and dimers (variation due to wall loss assumptions is indicated by white lines for simulated data). Panel d illustrates the frequency of peroxy radicals of different oxygenation state and carbon number. The inserts indicate radicals with 6 ("C6") and 5 ("C5") carbon atoms.

https://doi.org/10.5194/egusphere-2023-1415
Preprint. Discussion started: 26 July 2023

Slight underestimation of the formation of dimers in the range above 400 amu is observed (see Fig. 2 b). However, no sound explanation is available yet as the precursor molecules, highly oxidized RO_2, are assumed to be detected with highest efficiency and the formation of their dimeric products is considered to proceed close to the kinetic limit (~ 10^{-10} cm^3s^{-1}). Potentially, the underestimation of simulated dimer formation featuring high atomic mass might originate from ignored oxidation of closed shell dimers (of lower oxygen content), followed by autoxidation steps or by general underrepresentation of RO_2 concentration.

Since no flow tube data is available for benzene under elevated NO_x ($[NO_x]$ > 1 ppb_V) conditions, we used results from a steady state chamber setup to constrain the model (Garmash et al., 2020). While the monomer distribution is largely reproduced with regard to nitrate species formation, the dimer concentrations are underestimated by the model due to the scavenging of their precursor species, the peroxy radicals, by NO (see Supplementary Fig S15). The approach of stable closed shell species (i.e., closed shell products are not further oxidised) formation in the autoAPRAM-fw produces, compared to experiment, dimers of similar mass and composition. However, their abundance is considerably underestimated (~90%) under high NO_x conditions. Note that, in contrast to low NO_x conditions, the simulated HOM dimer fraction is much lower (dimer fraction ~ 2%). Detailed results under high NO_x conditions are discussed in the Supplementary (section SI "high NO_x conditions").

3.2 Partition to the particle phase

Alkoxy and peroxy radicals form upon oxidation of parent VOC. The radicals can undergo autoxidation and, as a consequence, isomerize to multi-functionalized molecules. The properties of these species deviate substantially from the parent VOC's. In order to compute their properties, we derived the potential molecular structures. Due to the fact that these molecules are often short lived, diverse (with regard to chemical composition and, most likely, isomeric variation), and only comprise a small fraction of the pool of reaction products, their structures have not yet been approached experimentally, besides a few exceptions (e.g., Tomaz et al., 2021). Thus, we base the structural suggestions on theoretic work and available knowledge on similar reaction classes (see Sect. 2.2 Setting up the gas-phase chemistry and Sect. 2.4 The molecular structures). The autoSMILES sub-module of the autoAPRAM-fw computes likely structures for all closed shell species. Potential structures of the peroxy radicals serve as an input. The applied approach is discussed in detail in the methods section. Partitioning of oxidation products between the gaseous and the condensed phases, in the presence of a condensation sink, is strongly affected by the species saturation vapor pressure. The p_{sat} is obtained by applying group contribution methods (e.g., O'Meara et al., 2014) to all structures. A quantum chemistry based statistical thermodynamics method, Conductor-like screening model for real solvents (COSMO-RS; Klamt, 1995; Klamt et al., 1998; Eckert and Klamt, 2002) is applied exclusively to a few species as it requires detailed analysis and extensive computational resources (see Sect. 2.5 Deriving the saturation vapor pressure).

Despite being an intensely studied molecule only few benzene oxidation experiments conducted under well defined, atmospherically relevant conditions which report SOA information can be found in the literature (Garmash et al., 2020; Ng

https://doi.org/10.5194/egusphere-2023-1415
Preprint. Discussion started: 26 July 2023

et al., 2007). In the present work we set up the ADCHAM model for the CALTECH (Keywood et al., 2004) and JPAC (Mentel et al., 2009) chambers to simulate seeded OH oxidation in the presence of UV light. Fig. 3 depicts simulation results and experimental data. Panels a, c and e compare reported (Garmash et al., 2020; Ng et al., 2007) and simulated aerosol mass formed and show calculated SOA mass yield based on the simulated data. Note that SOA mass yield is defined as SOA formed divided by benzene mass reacted. Values for aerosol mass formed agree well with the observations for panel a and c, representing low NO_x conditions ([NO] and [NO_2] < 1 ppt). Accordingly, the mass yields reported in literature were reproduced under reported conditions. Garmash et al. derived a maximum SOA mass yield of 40%, while we find 42% (12% to 71%); and Ng et al. observed a maximum mass yield of 37% which compares to 28% (14% to 42%) in the simulation of CALTECH chamber. For the high NO_x case shown in panel e, the SOA formation potential is underestimated (simulated mass yield of roughly 7% (3% to 7%) vs experimentally observed 26%). Ranges in simulated SOA yield result from different p_{sat}-estimation methods applied (see Sect. 2.5 Deriving the saturation vapor pressure). Fig. 3, panels b, d and f represent the contribution of MCM and autoAPRAM species, respectively, to the organic aerosol formed. In all three cases, the model suggests clear dominance (> 94 %) of the species formed via autoxidation. In the steady state experiment from JPAC chamber, the fraction of autoAPRAM species is highest (> 99%). Notably, the heterogeneous nucleation at the seed particle surface is initiated by species formed by autoxidation in all simulations (i.e., the autoAPRAM fraction approaches 100% at $t \rightarrow 0$ s after seed aerosol addition which corresponds to low reacted hydrocarbon in the CALTECH case). Further, note a conceptional difference, “steady state” vs “evolving chemistry” between experimental setups related to Fig. 3 panels a – b (i.e., resembling JPAC chamber) and c – f (i.e., resembling CALTECH chamber), respectively, which is highlighted by the evolution of the seed aerosol: while panel A shows an increase in seed aerosol upon production, followed by its decay, panels c and e represent an almost constant seed aerosol concentration present in chamber.

https://doi.org/10.5194/egusphere-2023-1415
Preprint. Discussion started: 26 July 2023

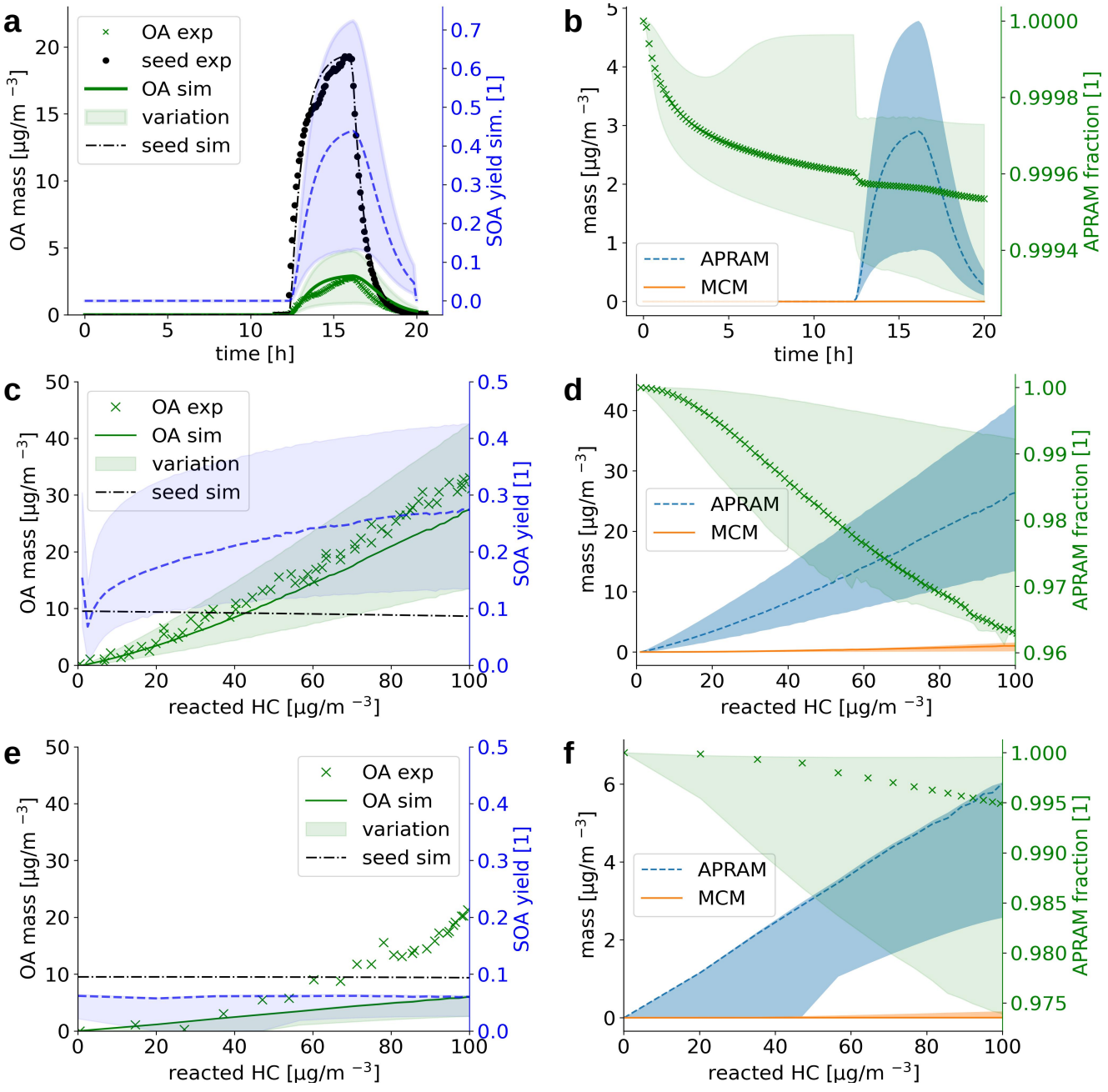

Fig 3: the simulation results when reproducing experimental chamber runs (panels a-b and c-f refer to JPAC chamber and CALTECH chamber, respectively). Panels on the left hand side (a,c & e) depict the organic aerosol formed (simulation: "OA sim"; experiment: "OA exp") as well as the seed aerosol present (simulation: "seed sim"; experiment: "seed exp"), respectively, shown on the left hand ordinate. The simulated SOA yield (dashed line; shaded area denotes the variation) is illustrated by the right hand ordinate. Results are shown as a function of reaction time (panels a & b) and reacted hydrocarbon (panels c, d, e & f). Panels b, d, and f contain computed information on the distribution of mass formed by MCM chemistry and by the autoxidation chemistry (APRAM), respectively. The right hand ordinate (panels b, d & f) shows the APRAM-species mass fraction of the particle-phase (green crosses). The variation of modeled data results from the different p_{sat} – determination methods applied.

https://doi.org/10.5194/egusphere-2023-1415
Preprint. Discussion started: 26 July 2023

3.3 Atmospheric implications:

VOC concentrations have been reported almost all around the globe. Benzene is a prototypical aromatic molecule which emission is related to mainly anthropogenic activities and is detected at high levels in many environments (Rocco et al., 2021; Misztal et al., 2015; Sekar et al., 2019). Besides benzene being toxic itself, its basic risk to health is via the oxidation in the atmosphere to contribute to the formation of nitrogen-containing species and secondary organic aerosol (World Health Organization, 2010). If emitted by a combustion process, benzene is mixed with NO_x. While NO_x, and in particular NO, concentrations decrease relatively quickly upon transport away from its source, benzene has an atmospheric lifetime of roughly 12 days (Blake and Blake, 2003). As a consequence, benzene is oxidized in the presence of varying NO_x mixing ratios.

To showcase effects of autoxidation chemistry on benzene atmospheric oxidation and SOA formation, the atmospheric chemistry transport and aerosol dynamics model ADCHEM was employed (Roldin et al., 2011). A more detailed description of the model setup is provided in the Methods section (2.6 Numeric simulations: ADCHAM & ADCHEM applications) and references therein. It was configured to simulate three air-mass trajectories arriving at Malmö, southern Sweden in the end of April, 2021. The simulations are named by the time the air-masses pass the city of Malmö: “9 am”, “10 am” and “11am” (UTC+1). For the selected cases, air masses from the Arctic Ocean between Greenland and Svalbard are transported over Scandinavia and the Baltic Sea before they arrive in Malmö 7-days later. Downwind Malmö the air masses are transported over Copenhagen and spend ~48 hours over the North Sea before they arrive near Brussels (see Supplementary Fig. S1). Results are analyzed in detail from one day upwind Malmö to the end of the simulation (Fig. 4). Based on emission inventories, the benzene concentrations remain low (< 0.1 ppb_V) until the calculated trajectories move over southern Sweden, and peaks over Copenhagen at ~ 0.7 ppb_V (Fig. 4, panel b; see also Figs. S2 and S3). Oxidants evolution, summarized in Panel a show a typical diurnal behaviour: OH level rises during the day. NO and NO_2, if emission is low, are converted to NO_3• radical by O_3. This process is suppressed during the daytime by photolysis: NO_3• and NO_2 are photolyzed to NO_2 and NO, respectively, which explains the source-independent increase in NO during daytime.

https://doi.org/10.5194/egusphere-2023-1415
Preprint. Discussion started: 26 July 2023

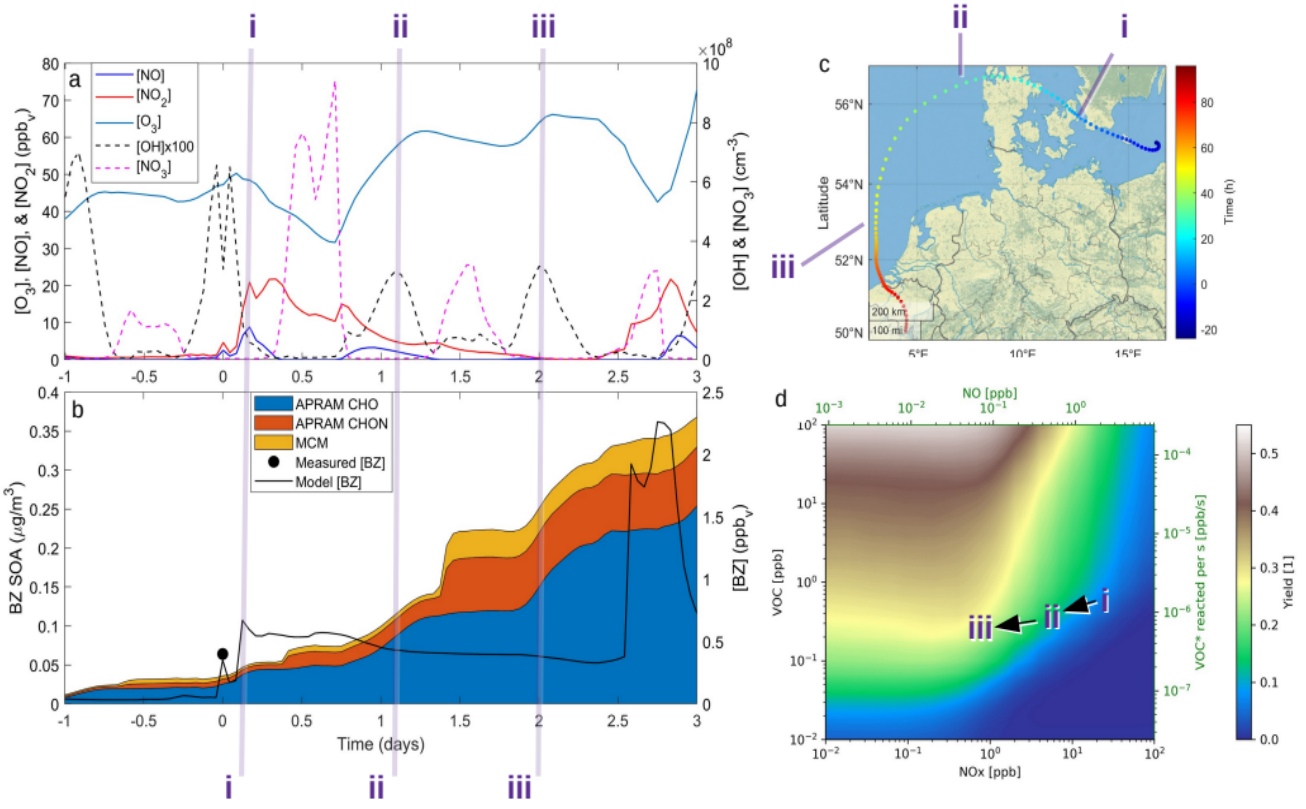

Fig. 4: ADCHEM results along the Case 3 ("11 am") air mass trajectory. Panel a shows the modelled gas-phase concentrations of NO, NO_2, O_3, OH and NO_3• from 1 day upwind (-1 day) to 3 days downwind Malmö. Note that OH concentration is scaled up by a factor of 100 to increase readability. Panel b shows the modelled benzene gas-phase concentrations (Model [BZ]) and the modelled benzene SOA mass concentrations of non-nitrate APRAM species (APRAM CHO), APRAM organonitrates (APRAM CHON) and MCM species. The modelled benzene is also compared with the observed benzene concentrations at the measurement station Dalaplan in Malmö (Measured [BZ]). The air mass trajectory path is displayed in panel c. Panel d illustrates the computed mass yield from OH oxidation in the presence of different levels of NO_x and VOC. Bottom and top abscissas depict NO_x and NO concentrations. VOC mixing ratio and VOC turnover are shown by the left and the right hand ordinate, respectively. The color code indicates the mass yield value. Note highlighted points in chemical space ("i", "ii" & "iii") in all panels.

Benzene, due to its aromatic structure, is oxidized only by OH at a considerable rate (Xu et al., 2020). The resulting peroxy RO_2 species drive the SOA formation during daytime via autoxidation chemistry (see "APRAM CHO"). Over Malmö and Copenhagen, the high NO concentrations partially suppress the autoxidation of peroxy radicals formed by OH oxidation of benzene, which result in less highly oxygenated organic molecules. The impact on aerosol mass yield and SOA composition are shown in the Supplementary (Figs. S4 – S6). As the air masses are transported away from the source (emissions of benzene and NO_x), the chemical system shifts to less NO_x-mediated autoxidation chemistry. The effect on SOA mass formed can be seen when comparing the situations "i", "ii" and "iii" in Fig 4, Panel b. Further, it is graphically illustrated in panel d which aims to depict the dependence of SOA mass yield on VOC (i.e., benzene), OH and NO_x.

https://doi.org/10.5194/egusphere-2023-1415
Preprint. Discussion started: 26 July 2023

There is a distinct increase in SOA mass after sunset which appears low as benzene levels are low; however, the ΔSOA gets more apparent after the air parcels have passed over the Oresund region (i.e. t = 0 days in Fig 4, panel b). During the first hours after the sunset during day 1 and 2 downwind Malmö/Copenhagen, rapid NO_3• oxidation of the intermediate MCM benzene oxidation product 4-nitrocatechol ($C_6H_5O_4N$), which is formed and accumulates in the gas-phase during the daytime, contribute to the formation of a highly oxygenated di-nitrate RO_2 species ($C_6H_5O_{11}N_2$). This results in substantial organonitrate SOA mass formation, composed mainly of organonitrate dimers ("CHON" Fig 4, panel b and Supplementary Figs S2 and S3, panel b). Those species, although highly oxygenated, are not considered HOM (according to definition by Bianchi et al., 2019) as the formation does not include autoxidation steps.

The trajectory model runs are contrasted by the more general picture of daytime benzene-SOA forming potential (see Fig. 4, Panel d). The SOA mass yield is calculated applying a box model (ADCHAM, see Sect. 2.6 Numeric simulations: ADCHAM & ADCHEM applications for details) mimicking the daytime atmospheric conditions and a range of VOC and NO_x mixing ratios. Generally, predicted yields vary between less than 1% for high NO_x and low VOC conditions, up to 50% under extreme conditions (high VOC and low NO_x). The computed mass yields show a slight increase with increasing NO as long as NO is low ([NO] < 0.1 ppb_V). Above roughly 0.1 ppb_V, the mass yield shows a distinct negative correlation with increasing NO. On the other hand, there is a positive correlation between the benzene turnover and yield. Note that these computed yields are highly dependent on OH concentration, despite being relatively insensitive regarding variations in seed aerosol properties, sunlight (neglecting the strong indirect effect via OH formation), methane concentration or O_3 (Fig Supplementary S7). Further, note that the OH and O_3 concentrations were set to constant values in these simulations in order to allow investigation of mass yields under various VOC/NO_x concentrations at a typical daytime OH level. This reflects the assumption that the VOC of interest is not dominating the OH sink. A strong variation in oxidants due to different VOC or NO_x levels would complicate the interpretation of individual data points as well as the comparability of mass yield results.

4 Discussion & Conclusions

Autoxidation chemistry is a key for understanding the atmospheric source of many multiply functionalized molecules and their potential partition to the condensed phase (Ehn et al., 2014). Applying reaction-rules of alkoxy- and peroxy radical chemistry enables to compile sets of chemical reaction equations in an almost automated fashion using the autoAPRAM-fw. In the present work we show that these reactions and their rate coefficients may be constrained against experimental data from flow tube and chamber to reproduce the part of the mass spectrum covered by HOM species within the limits of calculated error (typically less than 10% for relative concentrations of HOM species), including the distribution of peroxy radicals (see Fig 2). Predicting the species vapor pressure by group contribution methods proves successful to reproduce observed mass yields in seeded experiments found in the low NO regime (experimental: 40%(Garmash et al., 2020) and 37% (Ng et al., 2007) vs. simulated: 42% (range: 12% to 71%) and 28% (range: 14% to 42%), regardless of the experiment type.

https://doi.org/10.5194/egusphere-2023-1415
Preprint. Discussion started: 26 July 2023

In contrast, formation of condensed phase species is under-predicted under high NO conditions (experimental: 26% vs. simulated: 7%). Potential reasons for this discrepancy are diverse: a) The present approach neglects the oxidation of closed shell autoAPRAM species. Thus, if terminating reactions are dominating, the propagation of radical chemistry may be underrepresented. b) The prediction of the nitrate species' vapor pressure in the group contribution methods, generally, is considered less accurate compared to non-nitrated species as the experimental data is scarce (O'Meara et al., 2014). Reasons for few experimental data are, besides others, their high reactivity which makes the handling difficult. c) The high reactivity of NO_x species affects oxidation experiments in chambers and flow tubes as well. Accordingly, availability of high resolution CIMS data for nitrate species during VOC oxidation experiments is very limited which exacerbates model constraint. d) Formation of highly functionalized organic species in the presence of high NO mixing ratios likely does not proceed via RO_2 autoxidation as NO strongly limits the peroxy radical lifetime (Supplementary Fig S8). Thus, more fundamental work on nitrated species autoxidation and properties of the respective products will help to improve the model representation. Further note that reactive uptake of the oxidation products at the surfaces of the condensed phase is not modeled explicitly. Accordingly, the calculated SOA mass may be underrepresented in case reactive uptake is of importance, as could be the case for the product organonitrates.

The presence of high mixing ratios of NO and HO_2 poses additional challenges as their nitrate and ROOH yield by NO and H addition, respectively, is suggested to be very low for peroxy radicals attached to a C-ring (Xu et al., 2020). The yields of closed shell species during the RO_2 reaction with NO and HO_2 are predicted to be, besides the latter being highly uncertain, of the order of 0.1% and 1% respectively (Xu et al., 2020). Thus, the species allow for efficient NO_x and, likely but less certain, HO_x cycling. However, the molecular rearrangements of resulting alkoxy species are hard to predict (Vereecken and Peeters, 2010, 2009). In the present chemistry scheme, nitrate and ROOH yields in the range of 0.2% to 4% and 0.5% to 60% are applied. While the yields of $RONO_2$ species can be determined from CIMS data, the ROOH yields are less distinct as they can't be distinguished from species formed via other bi- or uni-molecular reactions, featuring the same composition.

Clearly, the model predicts potential, high mass yields of up to 55% from benzene oxidation under atmospheric-like daytime conditions (i.e. low NO_3● concentration; see Fig 4, panel d). Additional SOA formation is predicted from NO_3● oxidation of benzene-OH oxidation products shortly after sunset, resulting in the formation of highly oxygenated organonitrates. The modeled SOA mass yield positively correlates with increasing benzene turnover. This finding is supported by a recent work showing a positive correlation between benzene turnover and HOM formation (Garmash et al., 2020). The effect of NO on autoxidation is less uniform: at NO concentrations less than about 0.1 ppb_V, the yield positively correlates with NO, while at higher nitrogen oxide levels, there is a negative correlation. A similar trend was recently observed for thecyclohexene and α-pinene systems (Rissanen, 2018; Nie et al., 2023). A low NO concentration, due to high yield of alkoxy radicals, may speed up autoxidation. Note that RO H-shift rates are suggested to be orders of magnitude faster (about 10^3-10^7 s^{-1})(Vereecken and Peeters, 2010) compared to rate coefficients for peroxy radical H-shifts which are reportedly below 1 s^{-1} with few faster exceptions (Vereecken and Nozière, 2020; Crounse et al., 2013; Praske et al., 2018). H-shift rates for peroxy radicals in the range from 0.01 s^{-1} to 1.5 s^{-1} are applied in the current benzene-autoxidaiton scheme (see Supplementary section

https://doi.org/10.5194/egusphere-2023-1415
Preprint. Discussion started: 26 July 2023

"autoAPRAM – benzene scheme"). If NO concentration exceeds the level of 0.1 ppb_V, it starts to scavenge the RO_2 pool which forms the basis for peroxy radical autoxidation reactions and low-volatility dimer formation (see Supplementary Fig S8). For both RO and RO_2 species, H-shift rates strongly depend on the substitution and span of the H-shift (Otkjær et al., 2018).

A close to realistic atmospheric transport simulation, applying the complete chemistry scheme developed, suggests that condensable species formed by benzene autoxidation chemistry (added on top of MCM chemistry scheme by applying the autoAPRAM-fw) can have a significant share of the anthropogenic contribution to ambient organic aerosol mass. This fraction (up to 20%), likely, is over-predicted, as autoxidation chemistry, in the model, is still limited to a few VOC species: benzene, which is the focus of the work, as well as α-pinene, β-pinene, limonene and carene (Roldin et al., 2019). Additionally, the simulations for Malmö, Sweden, cover a period in April with cold Arctic air masses, which naturally limits the contribution of biogenic species.

Apparent mass yields from daytime autoxidation chemistry (determined from ADCHEM simulations) are similar to parametric simulations under comparable conditions (yields about 20%-52%; Supplementary Fig S4 – S6 and < 55%, respectively). There are differences between apparent mass yields in the atmospheric runs and mass yield from the parametric simulations: the parametric runs consider daytime conditions only. As a consequence the NO3● radical levels remain low and OH is the dominating oxidant. In the atmospheric simulations, OH oxidation-products of benzene accumulate during the day and are oxidized by NO_3● radicals in the dawn (see Supplementary Fig S9). Since OH is low while new SOA forms, the mass yield (ΔSOA/Δbenzene) can get very high as benzene is only oxidized by OH (Xu et. al., 2020). As a result, apparent mass yields of up to 1000% are observed during short periods in time. The simulated NO_3● oxidation of benzene-products seems to question the use of a general benzene mass yield based on OH oxidation experiments.

Direct comparison between atmospheric (simulation) data and mass yield simulations are generally difficult as characterizing parameters don't fully match (e.g., temperature, relative humidity). However, clearly, benzene and its intermediate oxidation products are oxidized under changing NO(x), OH● and NO_3● levels which on the one hand affects the formation of HOM species (in particular the dimer formation) and on the other hand impacts on the nitrogen-containing species' contribution to SOA. As the airmasses are transported away from hotspots of anthropogenic activity (i.e. emission sources of benzene and NO_x), the conversion of benzene to SOA via OH oxidation gets more effective due to a shift in the chemical regime towards less NO_x mediated chemistry (see Fig 4). The formation of SOA, during daytime, is as expected based on experimental findings (Ng et al., 2007; Garmash et al., 2020). In contrast, the increase of NO_3● at the dusk results in a distinct and timely limited increase in modeled SOA formation. This effect has not yet been investigated experimentally.

The authors assume that considering autoxidation chemistry for additional VOC species will most likely increase the formation of SOA and reduce the share of individual components. However, mixtures of VOC species may decrease the individual SOA yield via scavenging of the oxidants or by formation of higher volatility ROOR' (from RO_2 + RO_2') reaction products as shown for the system α-pinene – isoprene (McFiggans et al., 2019). On the other hand, it has been shown that

https://doi.org/10.5194/egusphere-2023-1415
Preprint. Discussion started: 26 July 2023

VOC mixtures may also increase mass yields significantly: Faiola et al. found augmentation of the aerosol formation by roughly 50% - 130% from real monoterpene-sesquiterpene mixtures emitted by stressed scots pine trees (Faiola et al., 2018). More recently, Voliotis et al. (2022) found that mixtures of α-pinene and o-cresol showed increased SOA formation compared to calculations based on additivity. Consequently, we think that a mechanistic representation of autoxidation chemistry is essential to improve the prognostic capacity in experiments and under atmospheric conditions. This includes the construction of models able to capture various aspects observed experimentally. We consider key parameters to be described in SOA production: a) radical production and sinks, b) chemical pathways (autoxidation of peroxy and alkoxy radicals; formation of accretion products and formation of closed shell species) leading to increased functionalization of the precursors and, c) partition of gas-phase molecules to the particle phase. Further, upon successful reproduction of experiments by means of modeling, reduction of the code to a reduced formal extent is inevitable to allow application in large scale models (Kaduwela et al., 2015). A mechanistic model-representation of key observations from experiments most likely is successful with regard to predictions in future changing atmospheres. Whereas, parameterized approaches that are based on few experimental data may fail as a result of prevailing conditions not resembling those in its experimental foundation. We are convinced that air quality forecasts, knowledge of the atmospheric chemistry and its impact on climate, and the basis for legislation can be significantly strengthened by following the approach introduced in this work.

Code availability

All codes to conduct the simulations of this work can be obtained from the corresponding author (LP) upon reasonable request.

Data availability

Data from flow tube, JPAC chamber (high/low NO_x) and CALTECH chamber (high/low NO_x) can be accessed online (https://doi.org/10.5281/zenodo.8087267). Data from ADCHEM atmospheric simulations are available upon request (office@pi-numerics.com).

Author contribution statement

LP, PR, MR, TK and MiB designed the research; LP, PR, MR, NH, CD, OG, CX, PZ, PC, BF, TGA, MeB, TK and MiB conducted the research; LP, PR, MR, MeB, MiB, NH, OG analyzed the data; LP and PR developed the models; LP, PR, MR and MiB wrote the paper.

https://doi.org/10.5194/egusphere-2023-1415
Preprint. Discussion started: 26 July 2023

Competing interests

Authors declare that they have no competing interests.

Acknowledgements

Austrian Science Funds (FWF), Grant No. J-4241 Schrödinger Programm

Swedish Research Councils FORMAS and VR (FORMAS project no. 2018-01745; VR project no. 2019-05006)

Crafoord foundation (project no. 20210969)

Academy of Finland, Grant No. 338171, 331207 and 336531

Academy of Finland (Center of Excellence, grant number 346369)

Acedemy of Finland (ACCC Flagship, 337549)

Jane and Aatos Erkko Foundation (JAES)

EU H2020 project FORCeS (821205)

European Commission Horizon Europe project FOCI (101056783)

This project has received funding from the European Research Council under the European Union's Horizon 2020 research and innovation programme under Grant No. 101002728.

University of Helsinki and Stockholm University (Autumn 2020 Arctic Avenue)

Computational resources were provided by CSC–IT Center for Science, Finland.

We would like to thank the Environmental Department City of Malmö for kindly providing benzene observations from the Dalaplan station in Malmö.

References

Ambient (outdoor) air pollution: https://www.who.int/news-room/fact-sheets/detail/ambient-(outdoor)-air-quality-and-health, last access: 8 November 2022.

BIOVIA COSMOconf: 2019, Dassault Systèmes, available at: http://www.3ds.com, last access: 20.2.2020.

BIOVIA COSMOtherm: Release 2019, Dassault Systèmes, available at: http://www.3ds.com, last access: 20.2.2020.

Particulate Matter (PM) Pollution: https://www.epa.gov/pm-pollution, last access: 8 November 2022.

Atkinson, R., Carter, W. P. L., Darnall, K. R., Winer, A. M., and Pitts, J. N.: A smog chamber and modeling study of the gas phase NOx-air photooxidation of toluene and the cresols, Int. J. Chem. Kinet., 12, 779–836, https://doi.org/10.1002/kin.550121102, 1980.

https://doi.org/10.5194/egusphere-2023-1415
Preprint. Discussion started: 26 July 2023

Berndt, T., Scholz, W., Mentler, B., Fischer, L., Herrmann, H., Kulmala, M., and Hansel, A.: Accretion Product Formation from Self- and Cross-Reactions of RO_2 Radicals in the Atmosphere, Angew. Chem. Int. Ed., 57, 3820–3824, https://doi.org/10.1002/anie.201710989, 2018.

Bianchi, F., Kurtén, T., Riva, M., Mohr, C., Rissanen, M. P., Roldin, P., Berndt, T., Crounse, J. D., Wennberg, P. O., Mentel, T. F., Wildt, J., Junninen, H., Jokinen, T., Kulmala, M., Worsnop, D. R., Thornton, J. A., Donahue, N., Kjaergaard, H. G., and Ehn, M.: Highly Oxygenated Organic Molecules (HOM) from Gas-Phase Autoxidation Involving Peroxy Radicals: A Key Contributor to Atmospheric Aerosol, Chem. Rev., 119, 3472–3509, https://doi.org/10.1021/acs.chemrev.8b00395, 2019.

Birdsall, A. W., Andreoni, J. F., and Elrod, M. J.: Investigation of the Role of Bicyclic Peroxy Radicals in the Oxidation Mechanism of Toluene, J. Phys. Chem. A, 114, 10655–10663, https://doi.org/10.1021/jp105467e, 2010.

Blake, N. J. and Blake, D. R.: TROPOSPHERIC CHEMISTRY AND COMPOSITION | VOCs: Overview, in: Encyclopedia of Atmospheric Sciences, Elsevier, 2438–2446, https://doi.org/10.1016/B0-12-227090-8/00422-X, 2003.

Bloss, C., Wagner, V., Jenkin, M. E., Volkamer, R., Bloss, W. J., Lee, J. D., Heard, D. E., Wirtz, K., Martin-Reviejo, M., Rea, G., Wenger, J. C., and Pilling, M. J.: Development of a detailed chemical mechanism (MCMv3.1) for the atmospheric oxidation of aromatic hydrocarbons, Atmos. Chem. Phys., 5, 641–664, https://doi.org/10.5194/acp-5-641-2005, 2005.

Compernolle, S., Ceulemans, K., and Müller, J.-F.: EVAPORATION: a new vapour pressure estimation methodfor organic molecules including non-additivity and intramolecular interactions, Atmos. Chem. Phys., 11, 9431–9450, https://doi.org/10.5194/acp-11-9431-2011, 2011.

Crounse, J. D., Knap, H. C., Ørnsø, K. B., Jørgensen, S., Paulot, F., Kjaergaard, H. G., and Wennberg, P. O.: Atmospheric Fate of Methacrolein. 1. Peroxy Radical Isomerization Following Addition of OH and O_2, J. Phys. Chem. A, 116, 5756–5762, https://doi.org/10.1021/jp211560u, 2012.

Crounse, J. D., Nielsen, L. B., Jørgensen, S., Kjaergaard, H. G., and Wennberg, P. O.: Autoxidation of Organic Compounds in the Atmosphere, J. Phys. Chem. Lett., 4, 3513–3520, https://doi.org/10.1021/jz4019207, 2013.

Daellenbach, K. R., Uzu, G., Jiang, J., Cassagnes, L.-E., Leni, Z., Vlachou, A., Stefenelli, G., Canonaco, F., Weber, S., Segers, A., Kuenen, J. J. P., Schaap, M., Favez, O., Albinet, A., Aksoyoglu, S., Dommen, J., Baltensperger, U., Geiser, M., El Haddad, I., Jaffrezo, J.-L., and Prévôt, A. S. H.: Sources of particulate-matter air pollution and its oxidative potential in Europe, Nature, 587, 414–419, https://doi.org/10.1038/s41586-020-2902-8, 2020.

Donahue, N. M., Epstein, S. A., Pandis, S. N., and Robinson, A. L.: A two-dimensional volatility basis set: 1. organic-aerosol mixing thermodynamics, Atmos. Chem. Phys., 11, 3303–3318, https://doi.org/10.5194/acp-11-3303-2011, 2011.

Eckert, F. and Klamt, A.: Fast solvent screening via quantum chemistry: COSMO-RS approach, AIChE J., 48, 369–385, https://doi.org/10.1002/aic.690480220, 2002.

Ehn, M., Thornton, J. A., Kleist, E., Sipilä, M., Junninen, H., Pullinen, I., Springer, M., Rubach, F., Tillmann, R., Lee, B., Lopez-Hilfiker, F., Andres, S., Acir, I.-H., Rissanen, M., Jokinen, T., Schobesberger, S., Kangasluoma, J., Kontkanen, J., Nieminen, T., Kurtén, T., Nielsen, L. B., Jørgensen, S., Kjaergaard, H. G., Canagaratna, M., Maso, M. D., Berndt, T., Petäjä, T., Wahner, A., Kerminen, V.-M., Kulmala, M., Worsnop, D. R., Wildt, J., and Mentel, T. F.: A large source of low-volatility secondary organic aerosol, Nature, 506, 476–479, https://doi.org/10.1038/nature13032, 2014.

https://doi.org/10.5194/egusphere-2023-1415
Preprint. Discussion started: 26 July 2023

Faiola, C. L., Buchholz, A., Kari, E., Yli-Pirilä, P., Holopainen, J. K., Kivimäenpää, M., Miettinen, P., Worsnop, D. R., Lehtinen, K. E. J., Guenther, A. B., and Virtanen, A.: Terpene Composition Complexity Controls Secondary Organic Aerosol Yields from Scots Pine Volatile Emissions, Sci Rep, 8, 3053, https://doi.org/10.1038/s41598-018-21045-1, 2018.

Fuller, R., Landrigan, P. J., Balakrishnan, K., Bathan, G., Bose-O'Reilly, S., Brauer, M., Caravanos, J., Chiles, T., Cohen, A., Corra, L., Cropper, M., Ferraro, G., Hanna, J., Hanrahan, D., Hu, H., Hunter, D., Janata, G., Kupka, R., Lanphear, B., Lichtveld, M., Martin, K., Mustapha, A., Sanchez-Triana, E., Sandilya, K., Schaefli, L., Shaw, J., Seddon, J., Suk, W., Téllez-Rojo, M. M., and Yan, C.: Pollution and health: a progress update, The Lancet Planetary Health, 6, e535–e547, https://doi.org/10.1016/S2542-5196(22)00090-0, 2022.

Garmash, O., Rissanen, M. P., Pullinen, I., Schmitt, S., Kausiala, O., Tillmann, R., Zhao, D., Percival, C., Bannan, T. J., Priestley, M., Hallquist, Å. M., Kleist, E., Kiendler-Scharr, A., Hallquist, M., Berndt, T., McFiggans, G., Wildt, J., Mentel, T. F., and Ehn, M.: Multi-generation OH oxidation as a source for highly oxygenated organic molecules from aromatics, Atmos. Chem. Phys., 20, 515–537, https://doi.org/10.5194/acp-20-515-2020, 2020.

Glowacki, D. R., Wang, L., and Pilling, M. J.: Evidence of Formation of Bicyclic Species in the Early Stages of Atmospheric Benzene Oxidation, J. Phys. Chem. A, 113, 5385–5396, https://doi.org/10.1021/jp9001466, 2009.

Goldstein, A. H. and Galbally, I. E.: Known and Unexplored Organic Constituents in the Earth's Atmosphere, Environ. Sci. Technol., 41, 1514–1521, https://doi.org/10.1021/es072476p, 2007.

Granier, C., Darras, S., Denier van der Gon, H., Doubalova, J., Elguindi, N., Galle, B., Gauss, M., Guevara, M., Jalkanen, J.-P., Kuenen, J., Liousse, C., Quack, B., Simpson, D., and Sindelarova, K.: The Copernicus Atmosphere Monitoring Service global and regional emissions (April 2019 version), https://doi.org/10.24380/D0BN-KX16.

Han, T., Ma, Z., Xu, W., Qiao, L., Li, Y., He, D., and Wang, Y.: Characteristics and source implications of aromatic hydrocarbons at urban and background areas in Beijing, China, Science of The Total Environment, 707, 136083, https://doi.org/10.1016/j.scitotenv.2019.136083, 2020.

Hinds, W. C. and Zhu, Y.: Aerosol technology: properties, behavior, and measurement of airborne particles, Third edition., Wiley, Hoboken, NJ, 1 pp., 2022.

Hyttinen, N., Otkjær, R. V., Iyer, S., Kjaergaard, H. G., Rissanen, M. P., Wennberg, P. O., and Kurtén, T.: Computational Comparison of Different Reagent Ions in the Chemical Ionization of Oxidized Multifunctional Compounds, J. Phys. Chem. A, 122, 269–279, https://doi.org/10.1021/acs.jpca.7b10015, 2018.

Hyttinen, N., Pullinen, I., Nissinen, A., Schobesberger, S., Virtanen, A., and Yli-Juuti, T.: Comparison of saturation vapor pressures of <i>α</i>-pinene + O₃ oxidation products derived from COSMO-RS computations and thermal desorption experiments, Atmos. Chem. Phys., 22, 1195–1208, https://doi.org/10.5194/acp-22-1195-2022, 2022.

Ingham, D. B.: Diffusion of aerosols from a stream flowing through a cylindrical tube, Journal of Aerosol Science, 6, 125–132, https://doi.org/10.1016/0021-8502(75)90005-1, 1975.

Jenkin, M. E., Saunders, S. M., and Pilling, M. J.: The tropospheric degradation of volatile organic compounds: a protocol for mechanism development, Atmospheric Environment, 31, 81–104, https://doi.org/10.1016/S1352-2310(96)00105-7, 1997.

https://doi.org/10.5194/egusphere-2023-1415
Preprint. Discussion started: 26 July 2023

Jenkin, M. E., Saunders, S. M., Wagner, V., and Pilling, M. J.: Protocol for the development of the Master Chemical Mechanism, MCM v3 (Part B): tropospheric degradation of aromatic volatile organic compounds, Atmos. Chem. Phys., 3, 181–193, https://doi.org/10.5194/acp-3-181-2003, 2003.

Jenkin, M. E., Young, J. C., and Rickard, A. R.: The MCM v3.3.1 degradation scheme for isoprene, Atmos. Chem. Phys., 15, 11433–11459, https://doi.org/10.5194/acp-15-11433-2015, 2015.

Jenkin, M. E., Valorso, R., Aumont, B., and Rickard, A. R.: Estimation of rate coefficients and branching ratios for reactions of organic peroxy radicals for use in automated mechanism construction, Atmos. Chem. Phys., 19, 7691–7717, https://doi.org/10.5194/acp-19-7691-2019, 2019.

Jimenez, J. L., Canagaratna, M. R., Donahue, N. M., Prevot, A. S. H., Zhang, Q., Kroll, J. H., DeCarlo, P. F., Allan, J. D., Coe, H., Ng, N. L., Aiken, A. C., Docherty, K. S., Ulbrich, I. M., Grieshop, A. P., Robinson, A. L., Duplissy, J., Smith, J. D., Wilson, K. R., Lanz, V. A., Hueglin, C., Sun, Y. L., Tian, J., Laaksonen, A., Raatikainen, T., Rautiainen, J., Vaattovaara, P., Ehn, M., Kulmala, M., Tomlinson, J. M., Collins, D. R., Cubison, M. J., E., Dunlea, J., Huffman, J. A., Onasch, T. B., Alfarra, M. R., Williams, P. I., Bower, K., Kondo, Y., Schneider, J., Drewnick, F., Borrmann, S., Weimer, S., Demerjian, K., Salcedo, D., Cottrell, L., Griffin, R., Takami, A., Miyoshi, T., Hatakeyama, S., Shimono, A., Sun, J. Y., Zhang, Y. M., Dzepina, K., Kimmel, J. R., Sueper, D., Jayne, J. T., Herndon, S. C., Trimborn, A. M., Williams, L. R., Wood, E. C., Middlebrook, A. M., Kolb, C. E., Baltensperger, U., and Worsnop, D. R.: Evolution of Organic Aerosols in the Atmosphere, Science, 326, 1525–1529, https://doi.org/10.1126/science.1180353, 2009.

Kaduwela, A., Luecken, D., Carter, W., and Derwent, R.: New directions: Atmospheric chemical mechanisms for the future, Atmospheric Environment, 122, 609–610, https://doi.org/10.1016/j.atmosenv.2015.10.031, 2015.

Keywood, M. D., Varutbangkul, V., Bahreini, R., Flagan, R. C., and Seinfeld, J. H.: Secondary Organic Aerosol Formation from the Ozonolysis of Cycloalkenes and Related Compounds, Environ. Sci. Technol., 38, 4157–4164, https://doi.org/10.1021/es035363o, 2004.

Klamt, A.: Conductor-like Screening Model for Real Solvents: A New Approach to the Quantitative Calculation of Solvation Phenomena, J. Phys. Chem., 99, 2224–2235, https://doi.org/10.1021/j100007a062, 1995.

Klamt, A., Jonas, V., Bürger, T., and Lohrenz, J. C. W.: Refinement and Parametrization of COSMO-RS, J. Phys. Chem. A, 102, 5074–5085, https://doi.org/10.1021/jp980017s, 1998.

Kroll, J. H. and Seinfeld, J. H.: Chemistry of secondary organic aerosol: Formation and evolution of low-volatility organics in the atmosphere, Atmospheric Environment, 42, 3593–3624, https://doi.org/10.1016/j.atmosenv.2008.01.003, 2008.

Kurtén, T., Hyttinen, N., D'Ambro, E. L., Thornton, J., and Prisle, N. L.: Estimating the saturation vapor pressures of isoprene oxidation products C₅H₁₂O₆ and C₅H₁₀O₆ using COSMO-RS, Atmos. Chem. Phys., 18, 17589–17600, https://doi.org/10.5194/acp-18-17589-2018, 2018.

Mattila, T., Kulmala, M., and Vesala, T.: On the condensational growth of a multicomponent droplet, Journal of Aerosol Science, 28, 553–564, https://doi.org/10.1016/S0021-8502(96)00458-2, 1997.

McFiggans, G., Mentel, T. F., Wildt, J., Pullinen, I., Kang, S., Kleist, E., Schmitt, S., Springer, M., Tillmann, R., Wu, C., Zhao, D., Hallquist, M., Faxon, C., Le Breton, M., Hallquist, Å. M., Simpson, D., Bergström, R., Jenkin, M. E., Ehn, M., Thornton, J. A., Alfarra, M. R., Bannan, T. J., Percival, C. J., Priestley, M., Topping, D., and Kiendler-Scharr, A.: Secondary

https://doi.org/10.5194/egusphere-2023-1415
Preprint. Discussion started: 26 July 2023

organic aerosol reduced by mixture of atmospheric vapours, Nature, 565, 587–593, https://doi.org/10.1038/s41586-018-0871-y, 2019.

Mentel, Th. F., Wildt, J., Kiendler-Scharr, A., Kleist, E., Tillmann, R., Dal Maso, M., Fisseha, R., Hohaus, Th., Spahn, H., Uerlings, R., Wegener, R., Griffiths, P. T., Dinar, E., Rudich, Y., and Wahner, A.: Photochemical production of aerosols from real plant emissions, Atmos. Chem. Phys., 9, 4387–4406, https://doi.org/10.5194/acp-9-4387-2009, 2009.

Misztal, P. K., Hewitt, C. N., Wildt, J., Blande, J. D., Eller, A. S. D., Fares, S., Gentner, D. R., Gilman, J. B., Graus, M., Greenberg, J., Guenther, A. B., Hansel, A., Harley, P., Huang, M., Jardine, K., Karl, T., Kaser, L., Keutsch, F. N., Kiendler-Scharr, A., Kleist, E., Lerner, B. M., Li, T., Mak, J., Nölscher, A. C., Schnitzhofer, R., Sinha, V., Thornton, B., Warneke, C., Wegener, F., Werner, C., Williams, J., Worton, D. R., Yassaa, N., and Goldstein, A. H.: Atmospheric benzenoid emissions from plants rival those from fossil fuels, Sci Rep, 5, 12064, https://doi.org/10.1038/srep12064, 2015.

Møller, K.H., Otkjær, R.V., Hyttinen, N., Kurtén, T. and Kjaergaard, H.G.: Cost-Effective Implementation of Multiconformer Transition State Theory for Peroxy Radical Hydrogen Shift Reactions. J. Phys. Chem. A, 2016 120 (51), 10072-10087, https://doi.org/10.1021/acs.jpca.6b09370

Møller, K.H., Otkjær, R.V., Chen, J., and Kjaergaard, H.G.: Double Bonds Are Key to Fast Unimolecular Reactivity in First-Generation Monoterpene Hydroxy Peroxy Radicals. J. Phys. Chem. A, 2020 124 (14), 2885-2896, https://doi.org/10.1021/acs.jpca.0c01079

Møller, K.H., Praske, E., Xu, L., Crounse, J.D., Wennberg, O.P., and Kjaergaard, H.G.: Stereoselectivity in Atmospheric Autoxidation. J. Phys. Chem. Letters 2019 10 (20), 6260-6266, https://doi.org/10.1021/acs.jpclett.9b01972

Molteni, U., Bianchi, F., Klein, F., El Haddad, I., Frege, C., Rossi, M. J., Dommen, J., and Baltensperger, U.: Formation of highly oxygenated organic molecules from aromatic compounds, Atmos. Chem. Phys., 18, 1909–1921, https://doi.org/10.5194/acp-18-1909-2018, 2018.

Molteni, U., Simon, M., Heinritzi, M., Hoyle, C. R., Bernhammer, A.-K., Bianchi, F., Breitenlechner, M., Brilke, S., Dias, A., Duplissy, J., Frege, C., Gordon, H., Heyn, C., Jokinen, T., Kürten, A., Lehtipalo, K., Makhmutov, V., Petäjä, T., Pieber, S. M., Praplan, A. P., Schobesberger, S., Steiner, G., Stozhkov, Y., Tomé, A., Tröstl, J., Wagner, A. C., Wagner, R., Williamson, C., Yan, C., Baltensperger, U., Curtius, J., Donahue, N. M., Hansel, A., Kirkby, J., Kulmala, M., Worsnop, D. R., and Dommen, J.: Formation of Highly Oxygenated Organic Molecules from α-Pinene Ozonolysis: Chemical Characteristics, Mechanism, and Kinetic Model Development, ACS Earth Space Chem., 3, 873–883, https://doi.org/10.1021/acsearthspacechem.9b00035, 2019.

Myrdal, P. B. and Yalkowsky, S. H.: Estimating Pure Component Vapor Pressures of Complex Organic Molecules, Ind. Eng. Chem. Res., 36, 2494–2499, https://doi.org/10.1021/ie950242l, 1997.

Nannoolal, Y., Rarey, J., and Ramjugernath, D.: Estimation of pure component properties, Fluid Phase Equilibria, 269, 117–133, https://doi.org/10.1016/j.fluid.2008.04.020, 2008.

Ng, N. L., Kroll, J. H., Chan, A. W. H., Chhabra, P. S., Flagan, R. C., and Seinfeld, J. H.: Secondary organic aerosol formation from <i>m</i>-xylene, toluene, and benzene, Atmos. Chem. Phys., 7, 3909–3922, https://doi.org/10.5194/acp-7-3909-2007, 2007.

Nie, W., Yan, C., Yang, L. et al.: NO at low concentration can enhance the formation of highly oxygenated biogenic molecules in the atmosphere. Nat Commun., 14, 3347 (2023). https://doi.org/10.1038/s41467-023-39066-4

https://doi.org/10.5194/egusphere-2023-1415
Preprint. Discussion started: 26 July 2023

O'Meara, S., Booth, A. M., Barley, M. H., Topping, D., and McFiggans, G.: An assessment of vapour pressure estimation methods, Phys. Chem. Chem. Phys., 16, 19453–19469, https://doi.org/10.1039/C4CP00857J, 2014.

Orlando, J. J. and Tyndall, G. S.: Laboratory studies of organic peroxy radical chemistry: an overview with emphasis on recent issues of atmospheric significance, Chem. Soc. Rev., 41, 6294, https://doi.org/10.1039/c2cs35166h, 2012.

Otkjær, R. V., Jakobsen, H. H., Tram, C. M., and Kjaergaard, H. G.: Calculated Hydrogen Shift Rate Constants in Substituted Alkyl Peroxy Radicals, J. Phys. Chem. A, 122, 8665–8673, https://doi.org/10.1021/acs.jpca.8b06223, 2018.

Praske, E., Otkjær, R. V., Crounse, J. D., Hethcox, J. C., Stoltz, B. M., Kjaergaard, H. G., and Wennberg, P. O.: Atmospheric autoxidation is increasingly important in urban and suburban North America, Proc. Natl. Acad. Sci. U.S.A., 115, 64–69, https://doi.org/10.1073/pnas.1715540115, 2018.

Riemer, N., Ault, A. P., West, M., Craig, R. L., and Curtis, J. H.: Aerosol Mixing State: Measurements, Modeling, and Impacts, Rev. Geophys., 57, 187–249, https://doi.org/10.1029/2018RG000615, 2019.

Rissanen, M. P., Kurtén, T., Sipilä, M., Thornton, J., Kangasluoma, J., Sarnela, N., Junninen, H., Jørgensen, S., Schallhart, S., Kajos, M., Taipale, R., Springer, M., Mentel, T. F., Ruuskanen, T., Petäjä, T., Worsnop, D. R., Kjaergaard, H. G., Ehn, M.: The formation of highly oxidized multifunctional products in the ozonolysis of cyclohexene, J. Am. Chem. Soc., 136, 15596– 15606, DOI: 10.1021/ja507146s, 2014.

Rissanen, M. P.: NO2 Suppression of autoxidation–inhibition of gas-phase highly oxidized dimer product formation, ACS Earth and Space Chem., 2, 1211– 1219, DOI: 10.1021/acsearthspacechem.8b00123, 2018.

Rissanen, M. P., Mikkilä, J., Iyer, S., and Hakala, J.: Multi-scheme chemical ionization inlet (MION) for fast switching of reagent ion chemistry in atmospheric pressure chemical ionization mass spectrometry (CIMS) applications, Atmos. Meas. Tech., 12, 6635–6646, https://doi.org/10.5194/amt-12-6635-2019, 2019.

Rocco, M., Dunne, E., Peltola, M., Barr, N., Williams, J., Colomb, A., Safi, K., Saint-Macary, A., Marriner, A., Deppeler, S., Harnwell, J., Law, C., and Sellegri, K.: Oceanic phytoplankton are a potentially important source of benzenoids to the remote marine atmosphere, Commun Earth Environ, 2, 175, https://doi.org/10.1038/s43247-021-00253-0, 2021.

Roldin, P., Swietlicki, E., Schurgers, G., Arneth, A., Lehtinen, K. E. J., Boy, M., and Kulmala, M.: Development and evaluation of the aerosol dynamics and gas phase chemistry model ADCHEM, Atmos. Chem. Phys., 11, 5867–5896, https://doi.org/10.5194/acp-11-5867-2011, 2011.

Roldin, P., Eriksson, A. C., Nordin, E. Z., Hermansson, E., Mogensen, D., Rusanen, A., Boy, M., Swietlicki, E., Svenningsson, B., Zelenyuk, A., and Pagels, J.: Modelling non-equilibrium secondary organic aerosol formation and evaporation with the aerosol dynamics, gas- and particle-phase chemistry kinetic multilayer model ADCHAM, Atmos. Chem. Phys., 14, 7953–7993, https://doi.org/10.5194/acp-14-7953-2014, 2014.

Roldin, P., Ehn, M., Kurtén, T., Olenius, T., Rissanen, M. P., Sarnela, N., Elm, J., Rantala, P., Hao, L., Hyttinen, N., Heikkinen, L., Worsnop, D. R., Pichelstorfer, L., Xavier, C., Clusius, P., Öström, E., Petäjä, T., Kulmala, M., Vehkamäki, H., Virtanen, A., Riipinen, I., and Boy, M.: The role of highly oxygenated organic molecules in the Boreal aerosol-cloud-climate system, Nat Commun, 10, 4370, https://doi.org/10.1038/s41467-019-12338-8, 2019.

Rolph, G., Stein, A., and Stunder, B.: Real-time Environmental Applications and Display sYstem: READY, Environmental Modelling & Software, 95, 210–228, https://doi.org/10.1016/j.envsoft.2017.06.025, 2017.

https://doi.org/10.5194/egusphere-2023-1415
Preprint. Discussion started: 26 July 2023

Saunders, S. M., Jenkin, M. E., Derwent, R. G., and Pilling, M. J.: Protocol for the development of the Master Chemical Mechanism, MCM v3 (Part A): tropospheric degradation of non-aromatic volatile organic compounds, Atmos. Chem. Phys., 3, 161–180, https://doi.org/10.5194/acp-3-161-2003, 2003.

Schraufnagel, D. E.: The health effects of ultrafine particles, Exp Mol Med, 52, 311–317, https://doi.org/10.1038/s12276-020-0403-3, 2020.

Sekar, A., Varghese, G. K., and Ravi Varma, M. K.: Analysis of benzene air quality standards, monitoring methods and concentrations in indoor and outdoor environment, Heliyon, 5, e02918, https://doi.org/10.1016/j.heliyon.2019.e02918, 2019.

Shiraiwa, M., Ueda, K., Pozzer, A., Lammel, G., Kampf, C. J., Fushimi, A., Enami, S., Arangio, A. M., Fröhlich-Nowoisky, J., Fujitani, Y., Furuyama, A., Lakey, P. S. J., Lelieveld, J., Lucas, K., Morino, Y., Pöschl, U., Takahama, S., Takami, A., Tong, H., Weber, B., Yoshino, A., and Sato, K.: Aerosol Health Effects from Molecular to Global Scales, Environ. Sci. Technol., 51, 13545–13567, https://doi.org/10.1021/acs.est.7b04417, 2017.

Sofiev, M., Soares, J., Prank, M., de Leeuw, G., and Kukkonen, J.: A regional-to-global model of emission and transport of sea salt particles in the atmosphere: SEA SALT EMISSION AND TRANSPORT MODEL, J. Geophys. Res., 116, https://doi.org/10.1029/2010JD014713, 2011.

Tomaz, S., Wang, D., Zabalegui, N., Li, D., Lamkaddam, H., Bachmeier, F., Vogel, A., Monge, M. E., Perrier, S., Baltensperger, U., George, C., Rissanen, M., Ehn, M., El Haddad, I., and Riva, M.: Structures and reactivity of peroxy radicals and dimeric products revealed by online tandem mass spectrometry, Nat Commun, 12, 300, https://doi.org/10.1038/s41467-020-20532-2, 2021.

Topping, D., Barley, M., Bane, M. K., Higham, N., Aumont, B., Dingle, N., and McFiggans, G.: UManSysProp v1.0: an online and open-source facility for molecular property prediction and atmospheric aerosol calculations, Geosci. Model Dev., 9, 899–914, https://doi.org/10.5194/gmd-9-899-2016, 2016.

Vereecken, L. and Nozière, B.: H migration in peroxy radicals under atmospheric conditions, Atmos. Chem. Phys., 20, 7429–7458, https://doi.org/10.5194/acp-20-7429-2020, 2020.

Vereecken, L. and Peeters, J.: Decomposition of substituted alkoxy radicals—part I: a generalized structure–activity relationship for reaction barrier heights, Phys. Chem. Chem. Phys., 11, 9062, https://doi.org/10.1039/b909712k, 2009.

Vereecken, L. and Peeters, J.: A structure–activity relationship for the rate coefficient of H-migration in substituted alkoxy radicals, Phys. Chem. Chem. Phys., 12, 12608, https://doi.org/10.1039/c0cp00387e, 2010.

Vereecken, L., Aumont, B., Barnes, I., Bozzelli, J. W., Goldman, M. J., Green, W. H., Madronich, S., Mcgillen, M. R., Mellouki, A., Orlando, J. J., Picquet-Varrault, B., Rickard, A. R., Stockwell, W. R., Wallington, T. J., and Carter, W. P. L.: Perspective on Mechanism Development and Structure-Activity Relationships for Gas-Phase Atmospheric Chemistry: PERSPECTIVE ON GAS-PHASE ATMOSPHERIC CHEMICAL KINETIC MECHANISM, Int. J. Chem. Kinet., 50, 435–469, https://doi.org/10.1002/kin.21172, 2018.

Voliotis, A., Du, M., Wang, Y., Shao, Y., Alfarra, M. R., Bannan, T. J., Hu, D., Pereira, K. L., Hamilton, J. F., Hallquist, M., Mentel, T. F., and McFiggans, G.: Chamber investigation of the formation and transformation of secondary organic aerosol in mixtures of biogenic and anthropogenic volatile organic compounds, Atmos. Chem. Phys., 22, 14147–14175, https://doi.org/10.5194/acp-22-14147-2022, 2022.

https://doi.org/10.5194/egusphere-2023-1415
Preprint. Discussion started: 26 July 2023

Wang, S., Wu, R., Berndt, T., Ehn, M., and Wang, L.: Formation of Highly Oxidized Radicals and Multifunctional Products from the Atmospheric Oxidation of Alkylbenzenes, Environ. Sci. Technol., 51, 8442–8449, https://doi.org/10.1021/acs.est.7b02374, 2017.

Weininger, D.: SMILES, a chemical language and information system. 1. Introduction to methodology and encoding rules, J. Chem. Inf. Model., 28, 31–36, https://doi.org/10.1021/ci00057a005, 1988.

Wollesen de Jonge, R., Elm, J., Rosati, B., Christiansen, S., Hyttinen, N., Lüdemann, D., Bilde, M., and Roldin, P.: Secondary aerosol formation from dimethyl sulfide – improved mechanistic understanding based on smog chamber experiments and modelling, Atmos. Chem. Phys., 21, 9955–9976, https://doi.org/10.5194/acp-21-9955-2021, 2021.

World Health Organization (Ed.): WHO global air quality guidelines. Particulate matter (PM2.5 and PM10), ozone, nitrogen dioxide, sulfur dioxide and carbon monoxide., Wold Health Organization, Geneva, 2021.

World Health Organization (Ed.): WHO guidelines for indoor air quality: selected pollutants, WHO, Copenhagen, 454 pp., 2010.

Xavier, C., Baykara, M., Wollesen de Jonge, R., Altstädter, B., Clusius, P., Vakkari, V., Thakur, R., Beck, L., Becagli, S., Severi, M., Traversi, R., Wehner, B., Sipilä, M., Kulmala, M., Boy, M., and Roldin, P.: Secondary aerosol formation in marine Arctic environments: A model measurement comparison at Ny-Ålesund, Aerosols/Atmospheric Modelling/Troposphere/Physics (physical properties and processes), https://doi.org/10.5194/acp-2022-200, 2022.

Xu, L., Møller, K. H., Crounse, J. D., Kjaergaard, H. G., and Wennberg, P. O.: New Insights into the Radical Chemistry and Product Distribution in the OH-Initiated Oxidation of Benzene, Environ. Sci. Technol., 54, 13467–13477, https://doi.org/10.1021/acs.est.0c04780, 2020.

Zhang, X., Cappa, C. D., Jathar, S. H., McVay, R. C., Ensberg, J. J., Kleeman, M. J., and Seinfeld, J. H.: Influence of vapor wall loss in laboratory chambers on yields of secondary organic aerosol, Proceedings of the National Academy of Sciences, 111, 5802–5807, https://doi.org/10.1073/pnas.1404727111, 2014.